2001-12

Ship detection performance predictions for next generation spaceborne synthetic aperture radars.

Simoì es, Marcus Vinicius da Silva

Monterey, California. Naval Postgraduate School

NAVAL POSTGRADUATE SCHOOL
Monterey, California

THESIS

SHIP DETECTION PERFORMANCE PREDICTIONS FOR NEXT GENERATION SPACEBORNE SYNTHETIC APERTURE RADARS

by

Marcus Vinícius da Silva Simões

December 2001

Thesis Advisor:	Philip A Durkee
Second Reader:	Jeffrey D.Paduan

THIS PAGE INTENTIONALLY LEFT BLANK

REPORT DOCUMENTATION PAGE			Form Approved OMB No. 0704-0188
Public reporting burden for this collection of information is estimated to average 1 hour per response, including the time for reviewing instruction, searching existing data sources, gathering and maintaining the data needed, and completing and reviewing the collection of information. Send comments regarding this burden estimate or any other aspect of this collection of information, including suggestions for reducing this burden, to Washington headquarters Services, Directorate for Information Operations and Reports, 1215 Jefferson Davis Highway, Suite 1204, Arlington, VA 22202-4302, and to the Office of Management and Budget, Paperwork Reduction Project (0704-0188) Washington DC 20503.			
1. AGENCY USE ONLY ***(Leave blank)***	**2. REPORT DATE** December, 2001	**3. REPORT TYPE AND DATES COVERED** Master's Thesis	
4. TITLE AND SUBTITLE: **Ship Detection Performance Predictions for Next Generation Spaceborne Synthetic Aperture Radars**			**5. FUNDING NUMBERS**
6. AUTHOR(S) Marcus Vinícius da Silva Simões			
7. PERFORMING ORGANIZATION NAME (S) AND ADDRESS (ES) Naval Postgraduate School Monterey, CA 93943-5000			**8. PERFORMING ORGANIZATION REPORT NUMBER**
9. SPONSORING / MONITORING AGENCY NAME (S) AND ADDRESS (ES) Brazilian Navy			**10. SPONSORING / MONITORING AGENCY REPORT NUMBER**
11. SUPPLEMENTARY NOTES The views expressed in this thesis are those of the author and do not reflect the official policy or position of the Department of Defense or the U.S. Government.			
12a. DISTRIBUTION / AVAILABILITY STATEMENT Approved for public release; distribution is unlimited.			**12b. DISTRIBUTION CODE**

13. ABSTRACT ***(maximum 200 words)***

Following success in other areas as a remote sensor, the spaceborne microwave image radars are assuming a notable position in the problem of ship detection for civilian and military purposes. This work will discuss the strong and weak points of Synthetic Aperture Radar (SAR) when used for ship detection. First, the thesis gives a brief description of SAR fundamentals, image processing and the parameters for ship detection. Second, the actual techniques, limitations, errors and some models used for ship detection are described. Finally, using a well-known and reliable ship detection model (Vachon et al., 1997), tested in the Canadian Ocean Monitoring Workstation and in some validation field programs, the new generation of spaceborne SARs, mainly RADARSAT 2, are analyzed for ship detection capabilities. During the analysis parameters like wind velocity, wind direction related to the antenna, satellite incident angle and Number of Looks are changed to study their influence on ship detection.

14. SUBJECT TERMS Synthetic Aperture Radar, Ship detection, Ship detection model, RADARSAR, ASAR, PALSAR			**15. NUMBER OF PAGES** 80
			16. PRICE CODE
17. SECURITY CLASSIFICATION OF REPORT Unclassified	**18. SECURITY CLASSIFICATION OF THIS PAGE** Unclassified	**19. SECURITY CLASSIFICATION OF ABSTRACT** Unclassified	**20. LIMITATION OF ABSTRACT** UL

NSN 7540-01-280-5500 Standard Form 298 (Rev. 2-89)
Prescribed by ANSI Std. 239-18

THIS PAGE INTENTIONALLY LEFT BLANK

Approved for public release; distribution is unlimited

SHIP DETECTION PERFORMANCE PREDICTIONS FOR NEXT GENERATION SPACEBORNE SYNTHETIC APERTURE RADARS

Marcus Vinícius da Silva Simões
Lieutenant Commander, Brazilian Navy
B.S.,Rio de Janeiro State University, 1985

Submitted in partial fulfillment of the
requirements for the degree of

MASTER Of SCIENCE IN PHYSICAL OCEANOGRAPHY

from the

NAVAL POSTGRADUATE SCHOOL
December 2001

Author: _____
Marcus Vinícius da S. Simões

Approved by: _____
Philip A. Durkee, Thesis Advisor

_____
Jeffrey D. Paduan, Second Reader, Co-Advisor

_____
Mary L. Batteen, Chairwoman
Department of Oceanography

THIS PAGE INTENTIONALLY LEFT BLANK

ABSTRACT

Following success in other areas as a remote sensor, the spaceborne microwave image radars are assuming a notable position in the problem of ship detection for civilian and military purposes. This work will discuss the strong and weak points of Synthetic Aperture Radar (SAR) when used for ship detection. First, the thesis gives a brief description of SAR fundamentals, image processing and the parameters for ship detection. Second, the actual techniques, limitations, errors and some models used for ship detection are described. Finally, using a well-known and reliable ship detection model (Vachon et al. 1997), tested in the Canadian Ocean Monitoring Workstation and in some validation field programs, the new generation of spaceborne SARs, mainly RADARSAT 2, are analyzed for ship detection capabilities. During the analysis parameters like wind velocity, wind direction related to the antenna, satellite incident angle and Number of Looks are changed to study their influence on ship detection.

THIS PAGE INTENTIONALLY LEFT BLANK

TABLE OF CONTENTS

LIST OF FIGURES

THIS PAGE INTENTIONALLY LEFT BLANK

LIST OF TABLES

THIS PAGE INTENTIONALLY LEFT BLANK

ACKNOWLEDGMENTS

First of all, I must thank Paris W. Vachon, PhD from the Canadian Center of Remote Sensing. Due to his priceless, patience and straight forward suggestions and advice this thesis was able to be finished.

Second, I would like to thank Professor Philip A. Durkee, my advisor from the Meteorology Department, for his friendly and well done guidance during this work and Professor Jeffrey D. Paduan, my co-advisor from the Oceanography Department for making, as a request of the Brazilian Navy, this thesis possible despite all the technical and bureaucratic problems involved.

I must thank as well, Professor Richard B. Olsen from the Physics Department, for being my main source of images, software, books and extra advice.

I must thank also, the Oceanographer Mike Cook for his teaching and help during not only this thesis work but also during my whole course.

Finally I wish to thank, my parents, sons, daughter and spouse for supporting twenty seven months of absence, everlasting hard work and endless studying of this son, father, husband and now, finally, author.

THIS PAGE INTENTIONALLY LEFT BLANK

I. INTRODUCTION

A. MOTIVATION

Having approximately 7,480 km (4650 miles) of coastline and 200 nautical miles of territorial sea, the total marginal sea area under the supervision of the Brazilian Navy totals the impressive amount of approximately 2,773,000 km^2. Maritime control and surveillance of this huge area requires all types of tools. To fulfill this task in time, with reliable accuracy, airborne and spaceborne microwave imaging sensors emerge as a valuable instrument. The advantages of this kind of tool include a regular repeating observation cycle, images free of cloud interference, high ground resolution (up to 3m in RADARSAT-2) and reliability. Synthetic Aperture Radars (SAR) have these essential features and offer a good trade-off between cost and benefit. In the future, use of SAR will be supported by a commercial remote sensing imaging boom. The new commercial SAR systems can supply images for specific requests with competitive cost and a potential for integration within modular ship monitoring systems. An increasing number of missions are being planned and executed as outlined in Table 1.

This thesis focuses specifically on three missions that will fly the next generation SAR sensors designed to fulfill various applications including ship detection. These sensors will be launched between 2001 and 2003 and include the following: the Japanese Space Agency Advanced Land Observing Satellite with the Phase Array type L-band Synthetic Aperture Radar (ALOS/PALSAR); the European Space Agency Environmental Satellite with an Advanced Synthetic Aperture Radar (ENVISAT/ASAR) and the Canadian Space Agency Radar Satellite 2 (RADARSAT 2).

Table 1. Planned SAR satellites missions [Updated from Olsen et al. (2000)]

Satellite (Owner/Operator)	Description	Key radar parameters			
		Swath width	Incidence angles	spatial res.	Modes
ENVISAT (USA) Launch jan 2002	ENVISAT will be the next satellite to be launched by the European Space Agency. The C-band ASAR instrument will be the first dual-polarised orbital SAR with a long term presence in space [3].	56-105 Km 56-105 km 405 km 405 km	15-45^0 15-45^0 17-42^0 17-42^0	30 m 30 m 150 m 1000 m	Image ALTPOL Wide Global
RADARSAT-2 (MDA/CSA) Launch 2003	This mission is designed to be yet another step closer to a fully commercial mission. Most of the investment is carried by the Orbital Sciences Subsidiary, Mac Donald Dettwiler, with the Canadian Space Agency as an anchor customer. The satellite will carry a C-band SAR that supports viewing to either side of the spacecraft track, high and low resolution modes and polarimetric capability.	100 km 150 km 170 km 70 km 50 km 500 km 300 km 25 km 25 km 50 km 20 km 10 km	20-50^0 20-45^0 10-20^0 50-60^0 37-48^0 20-50^0 20-46^0 20-41^0 30-41^0 30-50^0 30-40^0 30-40^0	28 m 28 m 28 m 20 m 9 m 100 m 50 m 28 m 9 m 3 m 3 m	Standard Wide Low Inc High Inc Fine ScanSAR Wide ScanSARNarrow Std QuadPod Fine QuadPod Triple Fine Ultra Fine Wide Ultra Fine Narrow
ALOS (NASDA) Launch 2003	Primarily a land observing mission, operating at L-band. The wide swath mode provides an imaging geometry that will provide good target to clutter ratios.	300 km	18-48^0	10-20 m 100 m	Image/Dual pol modes ScanSAR
TerraSAR (DLR/DASA/MMS/BNSC) [4]	TerraSAR is a commercial mission planned by a consortium of British and German industry. Current plans indicated a two-satellite system with X and L-band capability.	X-band: 10 km 20 km 100 km L-band: 40 km 60 km 200 km	 20-55^0 25-45^0 20-45^0 20-35^0 20-45^0 20-45^0	 1.6 m 3 m 15 m 9 m 9 m 30 m	 Spotlight Stripmap ScanSAR Quadpol Stripmap ScanSAR
COSMO/SKYMED	This is presently a mission concept developed under funding from the Italian Space Agency. The SAR system considered is the so-called SAR2000, an X-band radar capable of stripmap, spotlight and ScanSAR imaging.	3 km 30 km 120 km	< 45^0 < 45^0 < 45^0	1 m 3 m 25 m	Spotlight Stripmap ScanSAR
LightSAR (NASA/Industry)	This mission has been planned for some time by NASA, where an industry partner has been sought. Currently, discussions are being held with oil industry, to determine how a mission can be designed to meet that industry sector's requirements as well as NASA's science goals. The proposed radar is an L-band system with moderate resolution.				
Earth Watch (ESA/Industry)	The ESA Earth Watch programme is intended to be ESA's contribution towards a European Earth observation and monitoring system, in cooperation with private industry and organizations such as EUMETSAT. Industry proposals for mission concepts have been solicited, and several SAR missions are included. Further selections have not been confirmed to date.				

This thesis presents a technical review of one of these spaceborne SARs - the Canadian RADARSAR 2. This choice is due to the availability of commercial imagery, access to public information on the sensor, the success of the previous mission (RADARSAT-1), the set of technical improvements, and the suitability for the Brazilian Navy Project. Issues like ship tracking and target recognition that result from ship detectability improvements will be mentioned but not pursued in detail in this thesis. Expected results with new polarization improvements will also be mentioned but not analyzed in detail. This thesis will describe SAR operations and the physics of the ship detection problem.

B. THESIS OUTLINE

The first chapter describes the motivation and focus of this thesis. Chapter II presents some necessary SAR fundamentals and background needed to understand the ship detection problem. Constraints, limitations and explanation of system modes precedes the SAR imaging process in order to present a complete view of data acquisition through final image creation. Chapter III deals specifically with all facets of the ship detection problems, limitations, errors and techniques. The fourth chapter is the thesis core. All the results of quantitative improvements for the next family of spaceborne SARs are included in Chapter IV. Finally, Chapter V summarizes the results and conclusions focusing on SAR applicability to ship detection.

THIS PAGE INTENTIONALLY LEFT BLANK

II. BACKGROUND

A. THE SYNTHETIC APERTURE RADAR (SAR) FUNDAMENTALS

1. Basics

SAR systems.

A Synthetic Aperture Radar (SAR) is a Pulse-Doppler imaging radar that transmits short radio pulses in the microwave region of the spectrum. A SAR obtains resolution in range through travel time measurement, and uses Doppler shift of the backscattered signal to obtain resolution in azimuth as shown in Figure 1. The azimuth resolution is obtained using the concept of the synthetic antenna or synthetic aperture (Figure 2). A very long antenna is synthesized by moving a small antenna along a convenient path on a platform flight path or azimuth direction. The returning Doppler-shifted backscattered signal (amplitude and phase) is digitally processed to obtain information in the azimuth direction. The combination of time-resolved range and frequency-resolved azimuth results in a SAR image of target backscatter.

The SAR systems create a large amount of data necessitating extensive processing to produce images with the required resolution. This process is usually performed and stored in ground stations. In the early days of SAR observations, the processing was done optically, but due to the huge increase in computational power, all processing is currently done digitally.

The SAR technique was extended to use two antennas leading to the generation of three-dimensional images of the illuminated surface (Graham, 1974). This technique is

usually referred to as across track Interferometric Synthetic Aperture Radar (IFAR); however, IFAR is not the subject of this thesis.

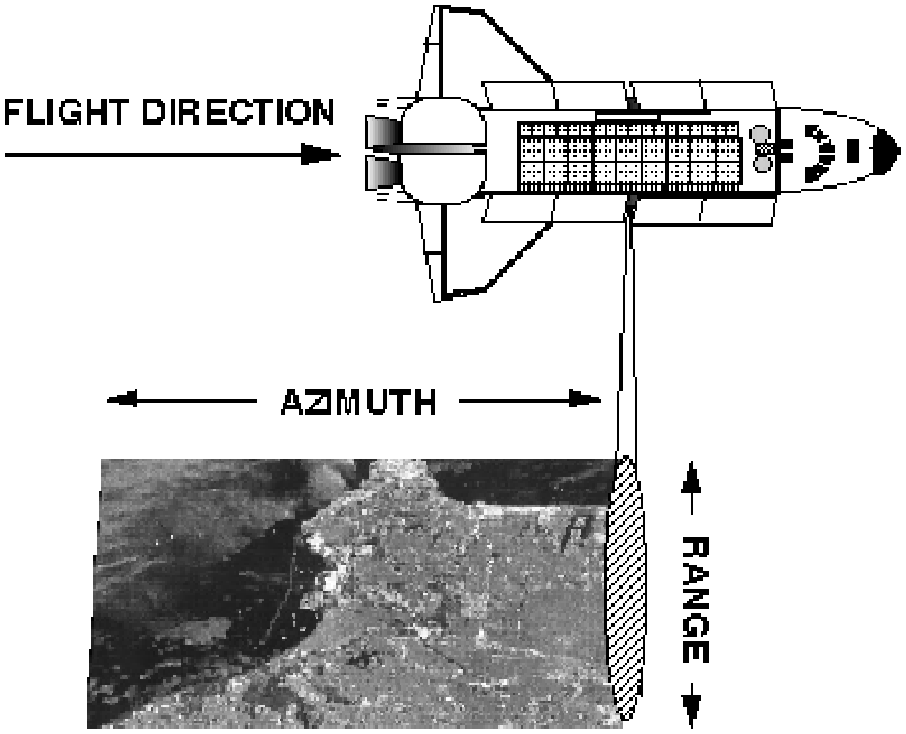

Figure 1. Azimuth and Range direction.
[From http://southport.jpl.nasa.gov/desc/imagingradarv3.html]

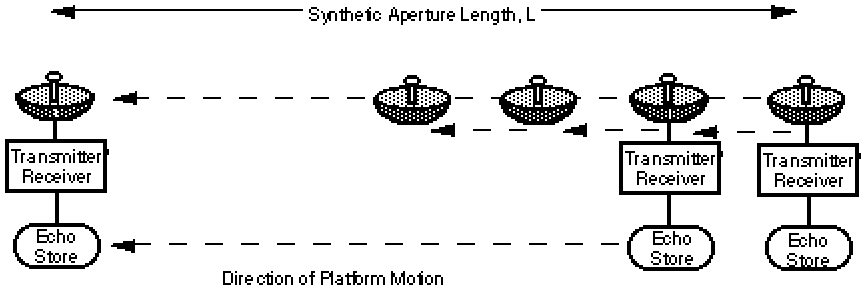

Figure 2. Azimuthal Synthetic Aperture
[From http://southport.jpl.nasa.gov/desc/imagingradarv3.html

2. SAR theory

The foundation of SAR theory is the synthesized antenna aperture to increase the along track or azimuthal resolution. The SAR theory is described in Curlander and McDonough (1992), and Elachi (1982). Figure 3 in three dimensions and Figure 4 in two dimensions summarize all terminology and geometry for SAR. A full, detailed description of SAR theory is beyond the scope of this work but some basics are needed to better understand the ship detection problem described below.

a) Azimuthal resolution

The well-known result shown below is described by Curlander and McDonough (1992) among others and began with the azimuth resolution for Side-Looking Aperture Radar (SLAR). The resolution is independent of the range and the radar wavelength, and improves with a smaller aperture, given by

$$r_{ap} = r_A = \frac{d_a}{2} \qquad [1]$$

where d_a is the antenna real aperture in azimuthal direction.

The corresponding resolution expression for an orbital SAR returns the complete result

$$r_{Ao} = \frac{R_e}{R_e + h}\frac{d_a}{2} \qquad [2]$$

where R_e is the earth radius and h is the platform altitude (Oliver, 1998).

b) Range resolution

The minimum separation between two resolvable points in SAR can be defined as the minimum range separation of two points that can be distinguished by the system as separate. For SAR sensors

$$r_y = r_g = \frac{\Delta R_s}{\sin h} = \frac{c t_p}{2 \sin h} \ , \qquad [3]$$

or after pulse compression techniques

$$r_g = \frac{c}{2 B_R \sin h} \ , \qquad [4]$$

where c is the light speed, ΔR_s is the resolution of the slant range, h is the incident angle between the radar beam and normal to the earth's surface and t_p is pulse duration.

c) Design considerations (constraints and limitations)

Below is a summary of the highlights of the critical design aspects of a SAR as an emitting and receiving sensor. Other technical construction constraints related to SARs are beyond the scope of this work.

(1) Choice of Pulse Repetition Frequency (PRF) or Pulse constraints.

The correct pulse duration is needed to achieve a reasonable range resolution and a sufficient echo signal to noise ratio (SNR). Chirp pulses and compression techniques are used to achieve the optimum PRF. This is a severe constraint in designing practical SARs due to the compromise between improving azimuth resolution and providing a wider swath width. Therefore, ignoring the earth's effect and orbit curvature for simplicity, we have from Robinson, (1985) the following:

$$\frac{2V}{d_a} = \frac{V}{r_A} \leq PRF \leq \frac{c}{2.W.\sin q} \quad , \qquad [5]$$

where *PRF* is Pulse Repetition Frequency, *W* is the swath width, *V* is the platform velocity, *?* is the angle between the slant direction and vertical (incident angle). The minimum PRF limitation is easier to visualize in terms of antenna theory because in those terms what determines the minimum PRF is the distance between successive array elements in the real antenna. If this distance is greater the λ/2, the so-called grating lobes (replications of the arrays' main lobe at increasing intervals on either side of the main lobe) will be produced.

(2) Sidelobes Minimization.

Stimson, 1998 states,

> Performance of a synthetic array radar may be degraded by both range sidelobes due to pulse compression and the sidelobes of the synthetic array. The sidelobes affect the radar maps in two different ways. First, the peaks of the stronger sidelobes may cause a string of progressively weaker false targets to appear on either side of a strong target. Second, the combined power of all sidelobes-called integrated sidelobe return-together with noise tends to fog or wash out the detail of the maps.

(3) Motion Compensation

Platform velocity and orbit are not perfectly constant as SAR theory assumes. The whole SAR concept is based on very slight signal phase changes over comparatively long periods. Therefore, it is essential that any motion during short periods be accounted for. A complete study of this error source is beyond the goal of this thesis, but the reader is referred to AGARD-LS-182 (1992).

(4) Antenna size limitations

The reduction in antenna size is limited by the operational necessity to generate a sufficiently powerful signal in order to obtain enough returned signal. A minimum value of the vertical antenna dimension is needed to focus the beam into the desired swath width. These two design constraints are other practical limitations to SAR system resolution improvements.

3. SAR operating modes

There are three operational modes of SAR systems: *STRIPMAP, SCAN AND SPOTLIGHT*, pictorially sketched in Figure 5 (Franceschetti, 1999). These *STRIPMAP* is the most popular which was developed and adapted into the following modes:

- *Squint forward and backward* – an array that, although it loses some azimuthal resolution, can execute applications like targeting/detection ahead of and behind the platform, and backscattering analysis of the properties of the illuminated surfaces with respect to the azimuth angle.
- Doppler beam sharpening provides high quality, continuously updating maps of large expansions of the surface with the penalty of reducing cross-range resolution distance Multilook mapping. This mode improves map quality by averaging out the scintillation of the radar returns.
- The *SCAN* mode tremendously increases the range swath dimension at the expense of azimuthal resolution while stepping the antenna beam to neighboring sub-swaths in range direction.

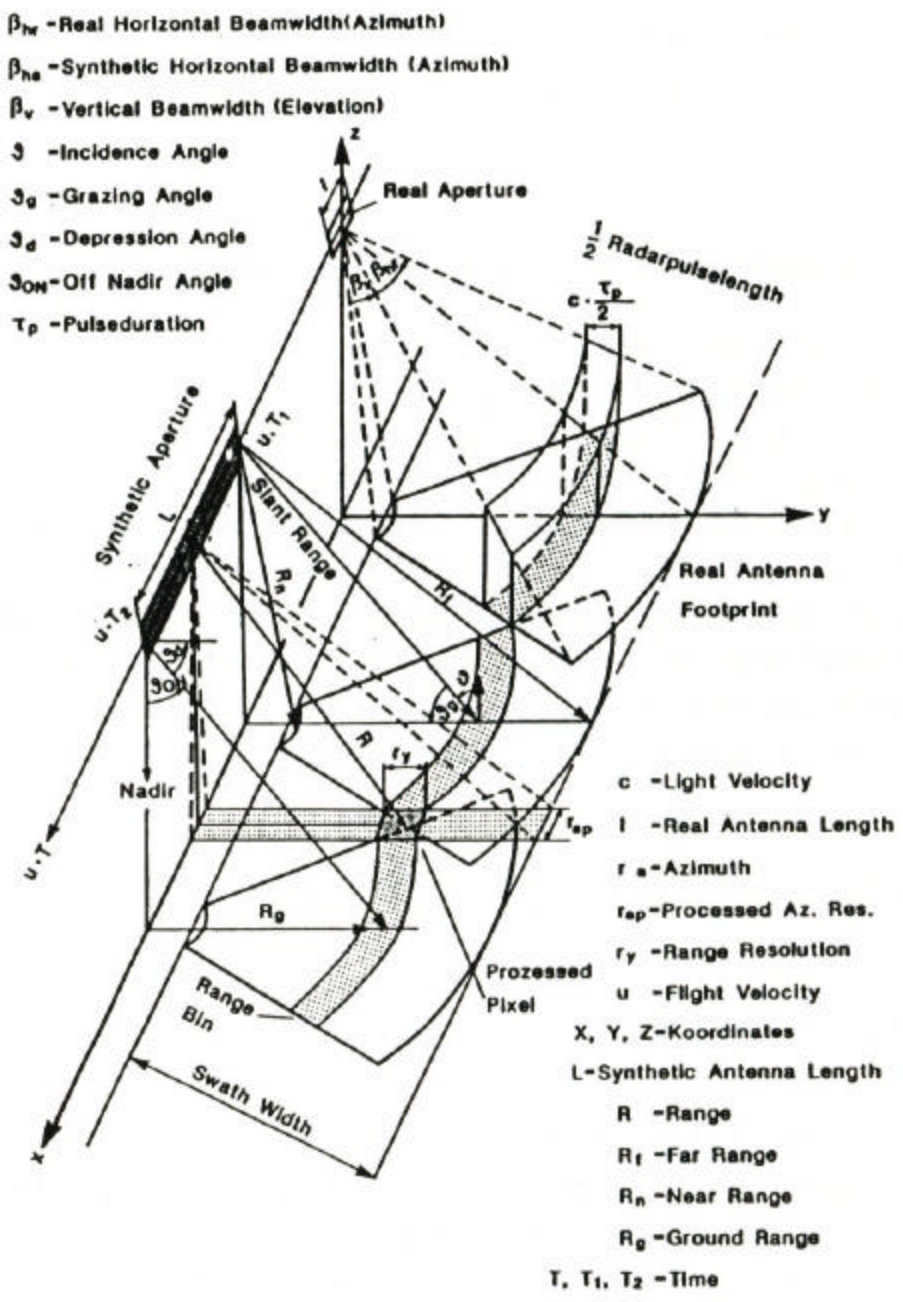

Figure 3. SAR terminology and geometry 1 [From AGARD-LS-182,1992]

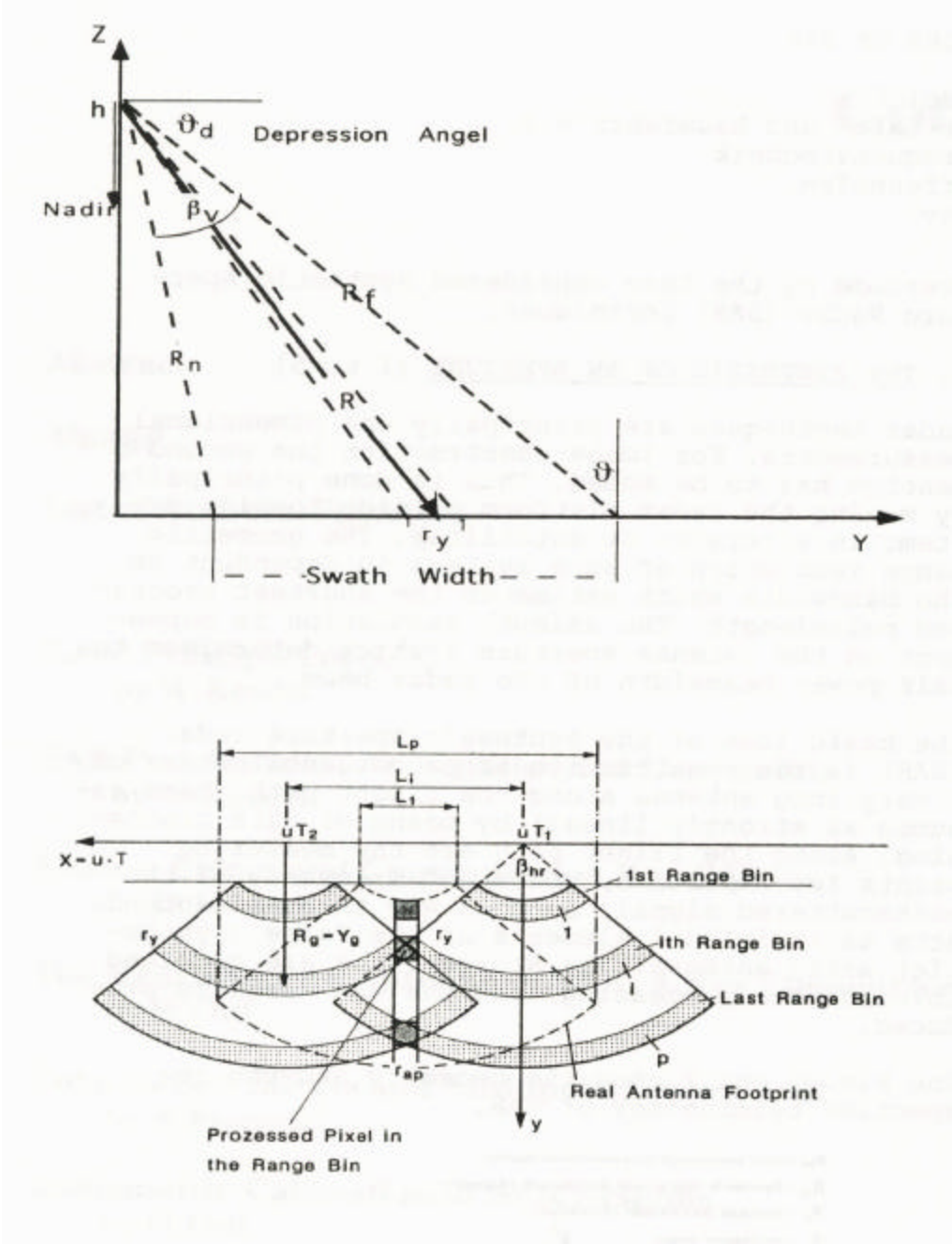

Figure 4. SAR terminology and geometry 2 [From AGARD-LS-182, 1992]

- The *SPOTLIGHT* mode is steered during overall acquisition time to illuminate the same area. A huge gain in azimuthal resolution is traded for a loss in coverage (small illuminated area along the sensor path).

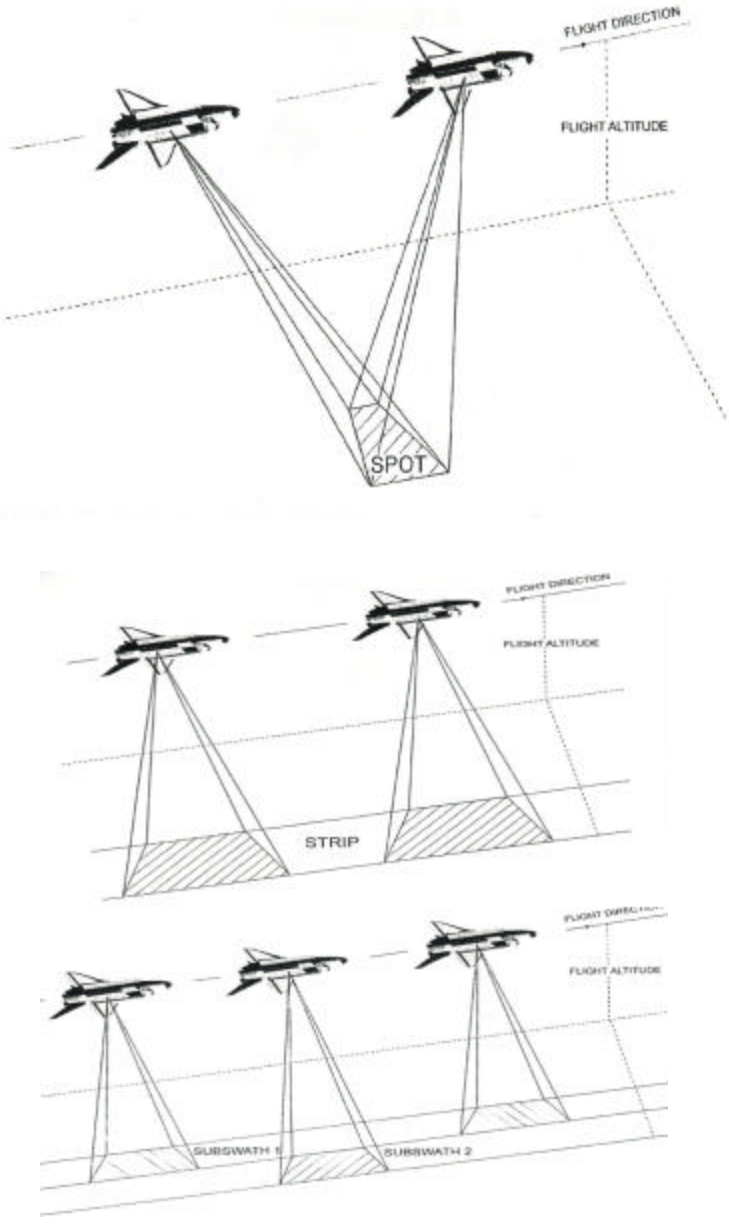

Figure 5. SAR operational modes [From Franchescetti, 1999]

B. SAR IMAGE PROCESSING

Using Stewart,(1985), the SAR image processing produces high spatial resolution in the azimuthal direction and high spatial resolution in range. Processing the radar signal in essence consists of taking a scattering time history at each range and convolving it with the point-target response to produce a line in the image. Using a continuous approach, Franceschetti (1999) states the two-dimensional processed SAR image expression as follows:

$$\hat{g}(x',r') = \iint g(x.r)\sin c\left[\frac{p}{\Delta x}(x'-x)\right]\sin c\left[\frac{p}{\Delta r}(r'-r)\right]dxdr \qquad [6]$$

where $\hat{g}(x,r)$ represents a two dimensional reflectivity scene pattern including the phase factor. Symbols *x* and *r* are the azimuthal and range direction respectively.

1. Geometric Resolutions

From Franceschetti (1999), also,

> Simply speaking, geometric resolution is the ability of the system to localize nearby objects. More precisely, the resolution length is the minimum spacing between two objects that are detected as separate entities, and are therefore resolved.

Both results for range and azimuthal were already presented in [1] and [3].

a) Focused x Unfocused

An “unfocused” SAR processing system is one which attains its along-track resolution by simple frequency filtering of the Doppler waveform. Higher azimuthal resolutions are only possible in a focused SAR system, which can account for the

variation in Doppler frequency of a target as it passes through the footprint resulting in the along-track resolution limit of half the antenna length.

2. Radiometric Resolutions

Franceschetti, (1999) defines radiometric resolution as " measure of the ability of the system to discriminate, or resolve, areas of different scattering properties. These are described by the reflectivity pattern ($g(x,r)$) of the illuminated surface."

Franceschetti, (1999) also states that changes in the reflective pattern are related to two different processes, one macroscopic (image intensity modulation proportional to $g(x,r)^2$ due to surface shape and/or its electromagnetic parameters as a function of space coordinates) and the other microscopic (essentially phase change due to surface roughness). A conventional definition of radiometric resolution given by Brooks and Miller, (1979) and Franceschetti, (1999) covers both microscopic and macroscopic process follows:

$$\Delta_{rd} = 10 * \log\left(1 + \frac{s}{m}\right) \qquad [7]$$

where m is the mean value and σ is the standard deviation of the image intensity referring to a distributed target of constant reflectivity. This states that adjoined areas with different intensities can be resolved, provided that their difference is larger than $\Delta_{rd.}$

3. Radiometric and Geometric Distortions

In practice, many factors can affect image quality by causing signal amplitude or phase modulation. The former is a consequence of antenna failure in stabilization

creating a change in the antenna point angle. Phase modulation is a consequence of an unpredicted change in the range between the object and the antenna, giving rise to an unknown receiving signal, which affects azimuthal pulse compression.

Oliver, (1998) summarizes that the *amplitude modulation* leads to radiometric distortions and increased side lobes, and phase modulation leads to image defocus, geometrical distortions (foreshortening, layover and shadow), radiometric distortions and increased sidelobe levels. Image defocus, radiometric distortion, and increased sidelobe levels restrict target detection and recognition capability. Geometrical distortions prevent direct pixel-to-pixel comparison, which is relevant to multichannel registration, target change detection, and direct image comparison. Motion Compensation (MOCO), made by accurate accelerometers and inertial navigational units mounted on the antenna, can reduce amplitude modulation effects. However, after this processes some residual unknown phase modulation still exists.

4. SAR Signal Statistics

In the case of a SAR scene, the only way to describe its roughness and density of scatters, for surface and volumetric scattering respectively, is in terms of statistical parameters. Data characterization throughout a probability density function (PDF) is a matter of compromise between simple models with few degrees of freedom and complex models with many degrees of freedom. Some well-known PDF with two-degrees of freedom like Weibull, lognormal, and the K distribution are used to statistically represent a SAR image. We will focus on the K-distribution since it is the PDF used in our ship detection model.

5. Speckle

The fluctuation in the receiving signal, known as *fading,* caused by the diverse nature of the return echo, generates a noise like grainy appearance on SAR imagery called *speckle*. It influences the ability to estimate image properties and thus is central to information retrieval from individual SAR images. Speckle has a noise like appearance, but it is not noise. An electromagnetic measurement can be useful, for example, in SAR interferometry. It can also be understood as an interference phenomenon in which the principal source of the noise like quality of the observed data is the distribution of the phase terms.

C. RELEVANT TOPICS IN SHIP DETECTION

1. Radar Cross Section (RCS)

The RCS describes the backscattering property of the target and depends on its size, shape and orientation as well as on wavelength and polarization of the incident signal (Skolnik, 2001). From the definition of RCS (σ) the cross section of an object that scatters equally in all directions (isotropic) is equal to its projected area.

a) Normalized Radar Cross Section (NRCS)

The quantity σ°, Radar Cross Section per Unit Area, provides a normalized parameter that can be used to describe RCS of the Sea independent of the radar illumination.

The normalized radar cross section (NRCS) is given by

$$\sigma^{o} = \sigma/A \quad [7]$$

where A is the area of a smooth surface that corresponds to the mean land or sea surface area contained within the radar's cell resolution. The illuminated area is a complicated

function of radar system parameters and is generally predictable as is described below in Section 3.

2. Ship Radar Cross Section

Ship reflectance is a complicated problem without a general solution. Skolnik (2001) proposed an empirical relation between displacement in tons and ship radar cross section. Vachon et al. (1997) using the Skolnik relationship developed the following linear regression between ship weight and length for the Bedford Institute of Oceanography Fleet and for some ships participating in the MARCOT'95:

$$\sigma = D = 0.08.L^{7/3} \quad [8]$$

where L is ship length and D is displacement.

Olsen et al. (2000) improved the above formula including the effect of incident angle using the same data from MARCOT'95

$$\sigma = D = R(\theta).0.08.L^{7/3} \quad [9]$$

where

$$R(\theta) = 0.78+0.11.\theta \quad [10]$$

All these formulations show that ship RCS is founded onobserved values and empirical methods.

3. Ocean Radar Cross Section

a) Nature of s° for Ocean and Incident Angle Dependency

The NRCS is sensitive to the character of the sea surface and is highly variable. It can change as much as 10 dB in a one-minute interval due to variations among measuring instruments and their calibration Long (2001). Therefore, measurement

errors and uncertainties tend to obscure the weak functional relationship between the wavelength (λ) and σ° for most incident angles. This relationship is a complicated function of incidence angle. For instance, at low incidence angle near the vertical, σ° is highly dependent on sea state and, for high incident angles, σ° is a strong function of λ. For horizontal polarization, the curve of σ° versus the grazing angle[1] θ for low frequencies is expected to be the same for microwaves except for a larger critical angle. Therefore, the curve for horizontal polarization might appear as in Figure 6.

b) Dependence of s° on Polarization

Polarization affects σ° for different surface conditions or for different wavelengths. From Long (2001) makes the following statements that hold for the ratio between σ°_{vv} (NRCS for vertical transmitted and vertical received polarization) and σ°_{hh} (NRCS for horizontal transmitted and horizontal received polarization):

1. The ratio increases with an increase in wavelength,
2. The ratio decreases with an increase in sea roughness, and
3. σ°_{hh} can exceed σ°_{vv} for heavy seas and small depression angles.

It should not be erroneously assumed from the above that under very rough conditions σ°_{vv} and σ°_{hh} are about equal for all incident angles.

c) Dependence of s° on Wind and Sea

Some of the sea surface characteristics known to influence various features of radar echos include the period and shape of the waves, the wave height, wind ripples, and the presence or absence of whitecaps and spray. However, observations

[1] 0° incidence angle from nadir (vertical) is equal to 90° grazing angle measured from horizontal plane

indicate that average and medium values of σ° increase as the sea becomes rougher for all grazing angles except for those near vertical incidence. Vachon et al. (1997) uses an empirical polarization ratio constructed by Unal et al. (1991) to transform from modeled values of σ°_{vv} to values of σ°_{hh} necessary for the ship length computation.

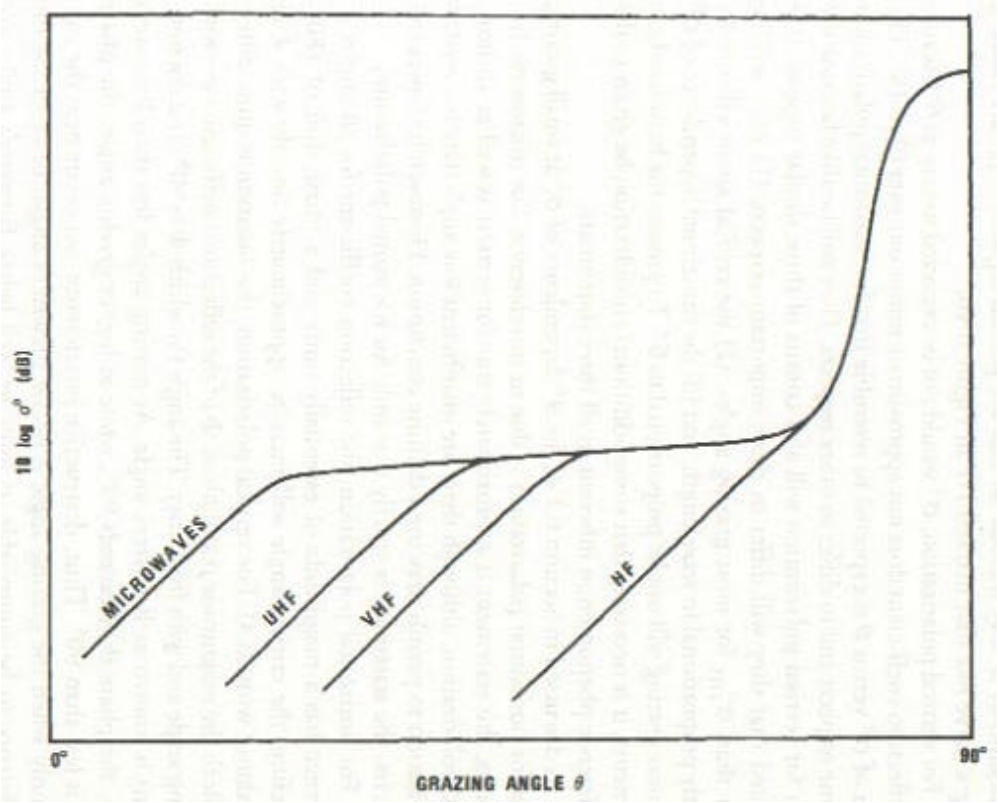

Figure 6. Shape of σ° versus Grazing Angle curves for horizontal polarization [From Long, 2001]

III. SHIP DETECTION PROBLEM

A. SHIP DETECTION APPROACHES

1. Ship-Generate Surface Waves (Wake detection)

Ship wake patterns exhibit various characteristics in SAR images under diverse environmental conditions. Wake structures in an image can be classified in three categories. First, surface waves generated by the ship; second, turbulent wakes or vortices containing relatively persistent but non-propagating currents visible in SAR imagery through the interaction of ambient waves with these surface currents (Lynden, 1988). Third, internal waves generated by the ship that are visible due to interaction with the short surface waves.

Ship wakes that are observed in SAR imagery are created by two mechanisms. First, variations of short waves (centimeters-scale) appearing as bright narrow "V" wakes are directly observed due to Bragg scattering in images; second, longer waves (decameter scale) forming the classical Kelvin-wake system are observed as they modulate the formation of Bragg scattering waves. Standard ship wake detection techniques exploit the first subcategory due to better pixel intensity (bright) response in SAR images. Some techniques (Rey et al. (1990), Copeland et al. (1995) and others) have been developed to use the Radon transform[2] in extracting linear features that are correlated with ship wakes.

Many specialists consider point target approaches a more efficient "pattern recognition" technique than wake detection. Wake detection techniques are very useful, after a candidate vessel is chosen, in order to confirm or reject the target as ship.

[2] A commonly used technique for finding lines in an image. Very robust in the presence of high levels of noise but lacking in differencing between short and long lines or end points of short lines.

Furthermore, in key applications like fisheries monitoring the vessels may often travel too slowly to generate significant wake signature (Olsen, 2000). This work will present a performance analysis of new spaceborne SARs using a point target detection approach.

2. Point Target Detection (Ship detection)

The main task of point target detection is to detect a single or a small cluster of pixels with the higher backscatter intensity from a ship within the background scene intensity. Generally, the background ocean has a lower backscatter intensity than ships. The ocean backscatter varies significantly with wind speed and wind direction relative to the SAR view angle, SAR beam incidence angle, and polarization of the returned power. The challenge of ship detection is unambiguously identifying the small number of bright ship pixels among the variable intensity of the background population of pixels.

3. Ship Detection Techniques

An intuitive approach to ship detection is to divide the scene into small frames assuming a single ocean backscatter value within each frame that determines a detection threshold for candidate vessels. The simplest method is to set the threshold intensity at *n* standard deviations above the image mean intensity. One variation of this technique uses two windows inside the image with different sizes. The windows are moved across the entire image using the larger window to compute the ocean background statistics while the smaller window is used for the actual target search.

Some more sophisticated parametric approaches fit a PDF (usually as a K-distribution) to the data and estimate the threshold based on the uncertainty level desired. One non-parametric method uses a probabilistic Neural Network approach. All these methods are designed to reach a balance between detection rate and the occurrence of

false alarms. To achieve this, some analysis methods are applied such as contrast measures, homogeneity tests, morphological filters, wake analyses, and combinations of these.

a) The Constant False Alarm (CFAR) method

The CFAR method sets a threshold for radars operating in a sea-clutter environment based on a PDF for the image ocean background intensities, integrated until a required significant level is reached. This significant level, $\eta_{c,}$ corresponds to a CFAR of 1-η_c for the intensity PDF

$$h_c = \int_0^{I_c} p(x)dx \qquad [8]$$

Two main problems arise from this method. The first problem is to find a PDF that fits an image intensity histogram. Second, I_c must be computed. Vachon (1997) uses η_c = 0.995 and p(x) is defined as a K-distribution for various order parameters.

THIS PAGE INTENTIONALLY LEFT BLANK

IV. NEXT GENERATION SHIP DETECTION EXPECTED RESULTS

The main question to be answered by a Ship Detection Model is what size of vessels can be detected in SAR imagery and how reliable is the detection under various observational conditions (Olsen, 2000). Secondarily, the model can indicate whether information like type, speed and heading can be retrieved from SAR imagery.

The key operational requirements for the next generation spaceborne SARs that are needed to improve ship detection are:

- Increase in resolution to be applied in target detection;
- increase in swath coverage to allow widespread ship monitoring and surveillance;
- larger incident angles (> 35°) to reduce ocean clutter and increase ship backscattering;
- greater coverage frequency in combination with higher resolution and programmable modes for selected areas.

Almost all of these desirable aspects will be flying on the next spaceborne SARs. The goal of this thesis is to apply, in a reliable model, the new specifications, mainly for resolution and incident angle, and retrieve the general performance behavior for different satellites and their different modes.

A. RELEVANT NEXT GENERATION SATELLITE PARAMETERS

This section gives a brief description of all three satellite and sensor characteristics and the launch schedule over the next 2-3 year window. Details for RADARSAT2, ENVISAT/ERS2 and ALOS/PALSAR SAR systems are summarized in the following sections

1. RADARSAT- 2

Table 2 presents RADARSAT-2 values for swath width, incident angles, Number of Looks, azimuthal and range spatial resolutions, multipolarization capability and others characteristics, like orbit parameters and coverage access using 500km swath width. Figure 7 shows the coverage pattern of all operational modes and Table 3 shows RADARSAT-2 inovations.

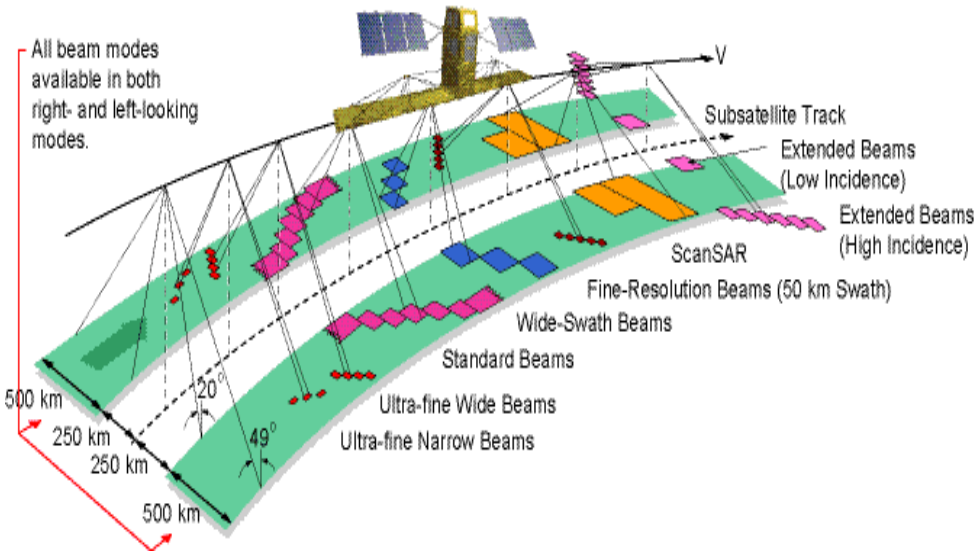

Figure 7. RADARSAR 2 Modes [From CCRS/RADARSAT- 2 site]

Table 2. RADARSAR 2 characteristics [From CCRS/RADARSAT- 2 site]

Standard Beam Modes	**Nominal Swath Width**	**Incidence Angles**	**Number of Looks**	**Approx. Resolution**
Wide	100km	20-50	1x4	25m x 28m
Low Incidence	150km	20-45	1x4	25m x 28m
High Incidence	170km	10-20	1x4	40m x 28m
Fine	70km	50-60	1x4	20m x 28m
ScanSAR Wide	50km	37-48	1x1	10m x 9m
ScanSAR Narrow	500km	20-50	4x2	100m x 100m
Standard Quad Pol.	300km	20-46	2x2	50m x 50m
Fine Quad Pol.	25km	20-41	1x4	25m x 28m
Triple Fine	25km	30-41	1	11m x 9m
Ultra-fine Wide	50km	30-50	3x1	11m x 9m
Ultra-fine Narrow	20km	30-40	1	3m x 3m

ORBIT CHARACTERISTICS

Altitude (average)	798 km
Inclination	98.6°
Period	100.7 minutes
Ascending Node	18:00 hrs
Sun-synchronous	14 orbits per day
Repeat Cycle	24 days

COVERAGE ACCESS USING 500km SWATH WIDTH

North of 70° H	Daily
North of 48° H	Every 1-2 days
Equator	Every 2-3 days

Table 3. RADARSAT-2 innovations [From Sanden (2001)]

INNOVATIONS	BENEFITS
GPS receivers onboard	±60-meter real-time position information
10 ms delay between imaging modes	Faster mode changes
Yaw-steering for zero-Doppler shift at beam center	Facilitates image processing
Higher downlink power density	3-metre minimum size antenna on ground allowing station portability and Lower "cost of entry" for new ground stations
3-meter ultra-fine resolution	Highest-resolution commercially available SAR
Left-and right-looking capability	Faster revisit time, 2000 km accessibility swath and Routine Antarctic mapping available
Fully polarimetric imaging modes	Enhanced capabilities for various applications
Solid-state recorders for onboard image storage	Higher reliability, faster image access and Simultaneous record and downlink

2. ENVISAT/ASAR

ASAR has five mutually exclusive modes of operation which could be classified in two categories: Global mission subdivided in to Global monitoring and Wave mode that have a low data rate and hence an operation capability up to 100% of the orbit, and regional mission subdivided in narrow swath modes, image mode and alternating polarization mode. Table 4 summarizes some operational parameters and Table 5 the mode's characteristics.

Table 4. ENVISAT/ASAR Operational Parameters [From ENVISAT Internet site]

Instrument Parameters	Image Mode	Alternating Polarization	Wide Swath	Global Monitoring	Wave Mode
Swath width	Up to 100 km	Up to 100 km	> 400 km	> 400 km	5 km vignette
Operation time	Up to 30 min per orbit			Rest of orbit	
Data Rate	Up to 100 Mbit/s			0.9 Mbit/s	
Power	1365 W	1395 W	1200 W	713 W	647 W

Table 5. ENVISAT/ASAR Modes [From ENVISAT Internet site]

ASAR Swathes Range Incidence Angle	**Swath Far**	**Width Range [km]**	**Near Incidence Angle**
IS1	108.4 - 109.0	14.1 - 14.4	22.2 - 22.3
IS2	107.1 - 107.7	18.4 - 18.7	26.1 - 26.2
IS3	83.9 - 84.3	25.6 - 25.9	31.1 - 31.3
IS4	90.1 - 90.6	30.6 - 30.9	36.1 - 36.2
IS5	65.7 - 66.0	35.5 - 35.8	39.2 - 39.4
IS6	72.3 - 72.7	38.8 - 39.1	42.6 - 42.8
IS7	57.8 - 58.0	42.2 - 42.6	45.1 - 45.3

3. ALOS/PALSAR

The Advanced Land Observing Satellite with a Phased Array type L-band Synthetic Aperture Radar (PALSAR) is the Japanese next generation spaceborne SAR. PALSAR uses L-band frequencies, different from RADARSAT and ENVISAT/ASAR, and has land observation as a major task and therefore has a variable beam elevation. The development of the PALSAR is a joint project between NASDA and Japan Resources Observation System Organization (JAROS). Its major specifications are listed in Table 6.

Table 6. ALOS/PALSAR specifications [From ALOS/PALSAR site]

Observation Mode	Fine Resolution Mode	ScanSAR Mode
Frequency	L-band	
Polarization	HH or VV (option: HV or VH)	
Spatial Resolution	10m (2looks)/20m (4 looks)	100m
Swath Width	70km	250-360km(3 - 5scans)
Off-nadir Angle	18 - 48deg.	
S/A	25dB	
NEσ^0	-25dB	

B. SHIP DETECTION MODEL APPLIED ON RADARSAT-1

Vachon et al. (1997) develops a model to study RADARSAT- 1 (C band HH polarization) performance for ship detection using the various beam modes. The model was validated with data acquired during the RADARSAT-1 ship detection/validation field program. Minimum detectable ship length is used as a Figure of Merit (FOM) for ship detection using RADARSAT-1 standard modes and ERS-1 modes. Validation of the model's key assumptions are provided, including those concerned with the hybrid C-band HH polarization ocean radar cross section model, the image probability density function and the ship radar signature model. This model is being updated by the Canadian Center of Remote Sensing (CCRS) and was applied and tested in the Ocean Monitoring Workstation - a system developed by Satlantic, Inc. with technical and financial support of CCRS, The Department of Fisheries and Oceans (DFO), Canadian Coast Guard (CCG), the Department of National Defense (DND) and the Canadian Space Agency (CSA). The OMW is designed to provide operational users of marine data with near-real time, value added ocean information derived from RADARSAT-1 SAR images (Vachon, 2000).

1. Model Assumptions

The model is based on three assumptions:

(1) the SAR image probability density function for ocean scenes can be described by the compound K-distribution model for sea clutter;

(2) the radar cross section of the ocean can be estimated given wind speed and beam geometry of C-Band radars;

(3) ship size is directly related to the radar cross section of the ship.

The model was developed using ERS-1 SAR data prior to RADARSAT-1 launch and was subsequently validated with RADARSAT-1 data.

2. SAR Ocean Scene Image Statistics

The compound K-distribution model is an empirical model for sea clutter that is applicable to high-resolution radars that resolve fine structure on the sea surface. Gaussian distributions do not fit for this kind of processes and the K-distribution does so due to the following observations from Rey, 1996:

> The envelope time history of a demodulated signal from an individual range cell shows fast fluctuations from pulse to pulse that is modulated by an underlying structure.
>
> The fast fluctuation component, or 'speckle', decorrelates from pulse to pulse with frequency agile signals but is correlated for between 5 and 10 ms with fixed frequency signals. This implies a large number of scatters within each illuminated patch. By applying the central limit theorem, the 'speckle' can be approximated by the Rayleigh distribution.
>
> The Slower modulation component is the local sea clutter mean level, which has a long temporal decorrelation period and is not affected by frequency agility. It characterizes the mean level variation of clutter, including clutter 'spikes', and its intensity is found to be gamma distributed;
>
> The gamma distribution is found in this model to be the first term in a Laguerre series expansion of the modulation PDF. The implication is that the non-Gaussian

nature of sea clutter seems to be due to more to scatter bunching by the sea wave structure than anything else.

The proposed distribution to describe the SAR PDF of image intensity is the multi-look intensity K-distribution (Oliver, 1993):

$$p(I)=\frac{2}{I}\left(\frac{LuI}{<I>}\right)^{(L+u)/2}\frac{1}{\Gamma(L)\Gamma(u)}K_{u-L}\left[2\left(\frac{LuI}{<I>}\right)^{1/2}\right] \quad [9]$$

where *p(I)* is the probability of the image intensity *I*, $<I>$ is the mean image intensity, L is the number of statistically independent looks, ν is an order parameter for the intensity modulation process, Γ is the gamma-function, K_{n-L} is the modified Bessel-function of *n-L* order.

Using the above PDF, we can now compute the critical intensity using [8] for any significant level, η_c. To retrieve the same results as Vachon et al. (1991) we use 0.995 significance level, a trapezoidal numerical routine for integration (0.005 and 0.01 intervals), and image mean $<I> = 1$.

3. RADARSAT- 1 SAR parameters

The RADARSAT-1 parameters are summarized on Table 7. The values are for nominal (near beam center) parameters for the 21 modes of the RADARSAT-1 SAR. ERS-1 values are also given for comparison.

4. Radar Cross Section of the Ocean

A physically-based model for the σ° relevant to RADARSAT-1 C-Band HH polarization is not available. Vachon et al. (1997), using Gower et al. (1993), based on Snoeij et al. (1991), incorporates empirical results from Unal et al. (1991) for backscatter

polarization ratio (PR^u). Table 8 lists the conversion factors to convert from a VV to HH Ocean Radar Cross Section polarization model.

Table 7. RADARSAR-1 parameters [From Vachon (1997)]

Beam Mode	Swath [km]	Looks (L)	θ[deg]	r_{az}[m]	r_{rg}[m]	$s°_{ne}$[dB]	Dchirp[km]
SI	100	3.1	*23.5*	27	24.2	-23	15.8
S2	100	3.1	*27.5*	27	20.4	-21	13.6
S3	100	3.1	*33.5*	27	*25.3*	-23	11.4
S4	100	3.1	37.0	27	23.4	-23	10.5
S5	100	3.1	39.0	27	22.1	-22	10.0
S6	100	3.1	*43.5*	27	20.3	-24	9.1
S7	100	3.1	47.0	27	19.1	-23	8.6
Fl	50	1	*38.5*	8.4	8.3	-23	10.1
F2	50	1	*40.5*	8.4	7.9	-22	9.7
F3	50	1	42.5	8.4	7.6	-23	9.3
F4	50	1	44.5	8.4	7.3	-24	9.0
F5	*50*	1	46.0	8.4	7.1	-23	8.6
W1	150	3.1	*25.5*	27	33.8	-22	14.6
W2	150	3.1	35.0	27	24.6	-22	11.0
W3	150	3.1	42.0	27	20.8	*-25*	9.4
EHI	*75*	3.1	*50.5*	27	18	-25	8.1
FH2	*75*	3.1	*51.5*	27	17.7	-25	8.0
EH3	*75*	3.1	*53.5*	27	17.3	*-25*	7.8
EH4	*75*	3.1	*55.5*	27	16.8	-23	7.6
FH5	*75*	3.1	57.0	27	16.6	-23	*7.5*
FH6	*75*	3.1	*58.5*	27	16.4	-23	7.3
ELI	170	3.1	16.5	27	39.1	-22	22.2
ERS-I	100	4.9	23.0	30.7	38.4	-24	14.2

This table includes the following parameters and modes: Sstandard; Ffine; W- wide; EH-extended high incidence; EL-extended low incidence; L is the number of independent looks; θ is the incidence angle ρaz is the azimuth resolution; ρrg is the ground-range resolution; σ°ne is the noise-equivalent clutter level; Dchirp is the ground-projected chirp length.

Table 8. Vertical to Horizontal C-Band (5.3 GHz) Polarization Ratios [From Unal et al. (1991)]

Inc.ang/ Wind(m/s)	20°	30°	45
2	1.05	2.07	4.78
4	0.79	2.37	5.25
6	0.65	2.57	5.47
8	0.56	2.70	5.59
10	0.51	2.80	5.66
12	0.49	2.88	5.71
14	0.49	2.95	5.75

The well-developed C-band VV (vertical/vertical) polarization model ($\sigma^{\circ}vv$) for ERS-1 scatterometer wind retrieval (the C band Models-CMOD series), was used here in conjunction with Table 8 ratios to produce the HH (horizontal/horizontal) RCS of the Ocean (σ°_{hh}) as showed below

$$\sigma^{\circ}_{hh} = \sigma^{\circ}_{vv} - PR^{u} \qquad [10]$$

5. Radar Cross Section of Ships

Based on Skolnik (2001), Vachon et al. did a linear regression between ship weight and length for the Bedford Institute of Oceanography (BIO) fleet and some ships participating in the military exercise MARCOT'95, resulting in the following empirical relation:

$$\sigma_{ship} = D = 0.08.L^{7/3} \qquad [11]$$

where σ_{ship} is the ship radar cross section, *'D'* is the ship displacement and *'L'* ship length.

The model can then determine the ship detectability by a SAR based on a ship scale parameter. Knowing the critical intensity (I_c) of the relevant PDF from [9] and the ocean normalized cross section (σ°) from [10], the model can determine the corresponding minimum point target RCS for detection at a chosen probability level as

$$s = I_c s^{0} r_{az} r_{rg} \qquad [12]$$

where ρ_{az} is the satellite azimuthal resolution cell size and ρ_{rg} is the ground range resolution cell size.

6. Ship Length computation

Combining [11] and [12] we have the minimum detectable ship length as a function of the Ocean RCS, resolutions and critical intensity, as follows:

$$L = (I_c s^{0} r_{az} r_{rg} / 0.08)^{3/7} \qquad [13]$$

Applying this results to RADARSAT-1 data, Vachon et al. (1997) produced results for S1, S3 and S7 RADARSAT-1 modes and ERS to test the model, considering -23 dB as the RADARSAT-1 noise equivalent normalized radar cross section (σ_{NE}) with clutter noise ratio (CNR) = $\sigma°/\sigma_{NE}$ and σ_{NE} = –24 dB for ERS.

7. Vachon et al. Ship Detection Model Results

Some results for this model for RADARSAR 1 mode S1, S3, S7 and ERS SAR are presented in Figure 8. Each plot shows the minimum detectable ship length as a function of wind speed using equation [13] where solid lines represent the Upwind direction (ie, ϕ=0, the largest $\sigma°$, hence the worst case – least detectable due to a bright background) while dashed lines represent the Crosswind direction (ie,ϕ=90°, the smallest $\sigma°$, hence the best case). The three curves represent variation of the order parameters for K-distribution from top to bottom: ν= 4, 10, 8 (ie, from worst to best case). To facilitate comparison among the various RADARSAT-1 beams and modes, Vachon et al. (1997) defines a FOM for ship detection using Upwind ϕ = 0° direction, wind velocity U = 10 m/s, and order parameter ν = 4. The resulting plot is shown in Figure 9.

8. Vachon et al. results validation

A validation field program was held in March/April 1996 to provide quantitative information to validate the ship detection model. Some of the elements used to validate the model are showed in Vachon et al. (1997) and summarized here. They include acquisition of wind and wave data from two buoys, acquisition of nine RADARSAT-1 SAR scenes in various modes, placement of ship near the buoys at the time of RADARSAT-1 SAR passes, and surveillance flights over the area to identify additional ship targets on an opportunity basis.

After RADARSAT-1 calibration and SAR data processing, Vachon et al. (1997) concludes,

> We validated some of the ship detection model assumptions using our calibrated RADARSAR SAR data. In particular, we show that there is excellent agreement between the observed RADARSAT-1 SAR cross section and those predicated by the hybrid model. Furthermore, the K-distribution in shown to be a suitable PDF for RADARSAT-1 SAR ocean images. We also show that our very simple ship length-dependent cross section model is within the correct order of magnitude

C. SHIP DETECTION MODEL APPLIED TO NEXT GENERATION SPACEBORNE SAR PARAMETERS

1. Some Considerations

From Vachon et al. (1997), we have some important statements about the radar cross section of the ship. They are: "…For the ship considered, we find that our simple relationship is within 20dB, but that the anomaly tends to increase with increasing incidence angle", and more " …Although we have not considered ship orientation at all in this analysis, use of the best fit line to our data allows recovery of the vessel length to

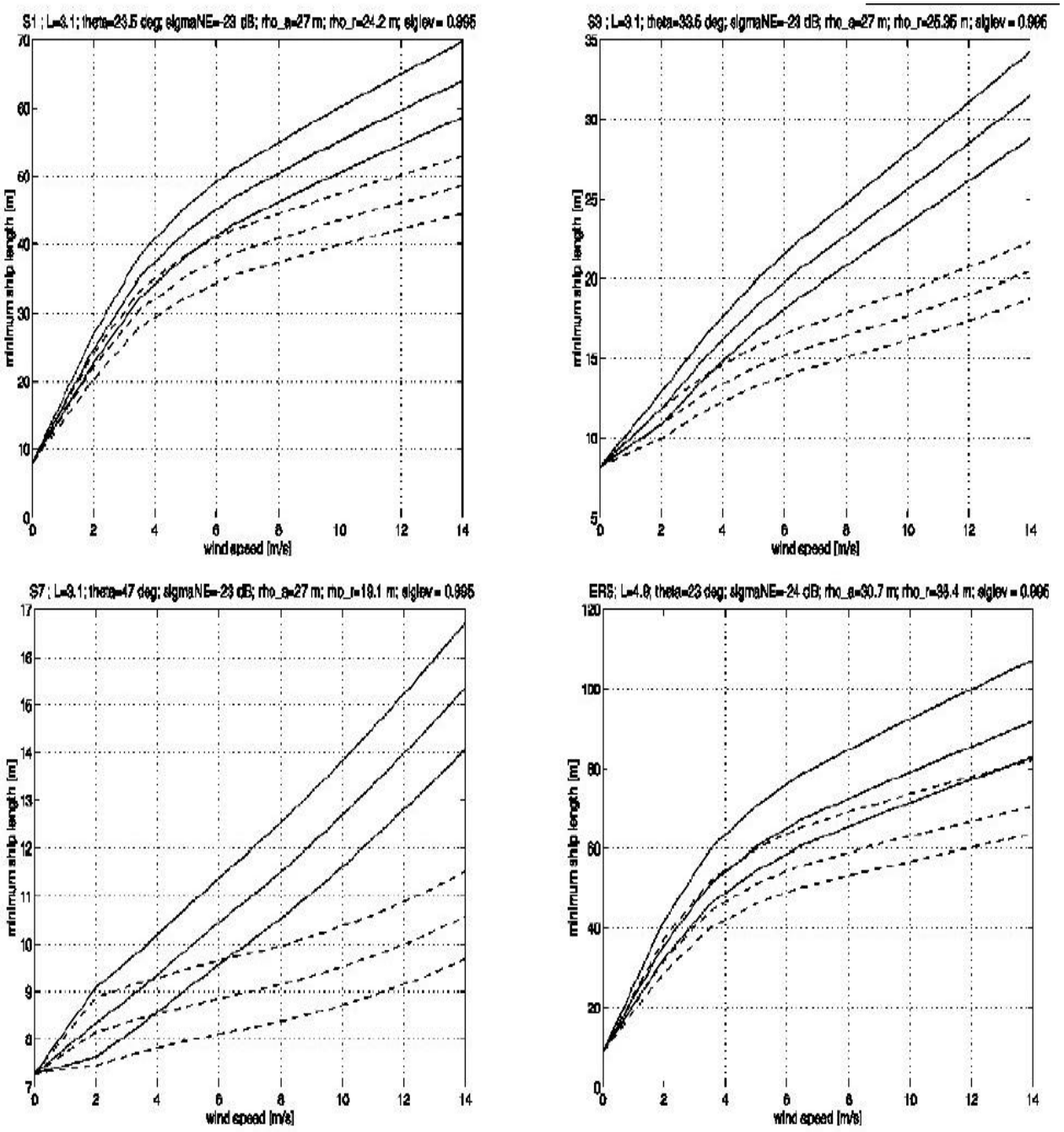

Figure 8. Vachon et al. (1997) results for ship length versus wind speed for RADARSAT-1 S1, S3, S7 and ERS

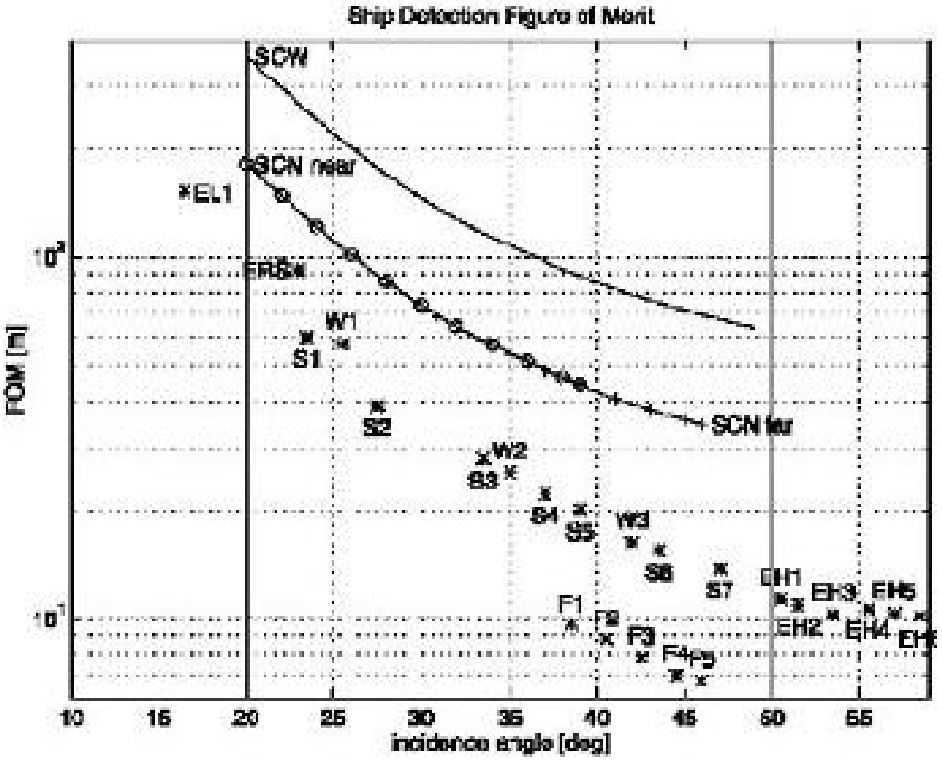

Figure 9. Figure of Merit from Vachon et al. (1997)

within 20% based on the measured ship cross section alone. It is apparent that our simple ship model will tend to underestimate the ship detectability."

Due to the good results presented and supported by Vachon et al. (1997), the model is used here to describe the physical processes that limit ship detection and to quantify the ship detection improvements that can be expected in the next generation spaceborne SARs.

Unal's et al. (1991) table is used as reference and including only values linearly interpolated inside the table wind range (except for mode S7 where an linear

extrapolation to 47° of incident angle) The computations begin at 2 m/s wind velocity for to two reasons. First, due to a lack of Unal et al. (1991), values inside this interval to confirm our values. Secondly, because our computed curves have a better agreement with Vachon et al. (1997), only results between the 2 to 14 wind speed interval are included here.

2. Reproducing Results with Vachon et al. model:

The Vachon et al. (1997) model is reproduced here using RADARSAT-2 specifications and the same image parameters used for RADARSAT-1 except for resolution. All considerations taken in IV-C-1 were generated during this computation due to a small difference in length values and a more linear result for all RADARSAT-2 and ERS modes. Figures 10,12,14 and 16 from below with Figure 8.

3. Expected Result for all RADARSAT 1 modes kept in RADARSAT-2

All four cases resulting from [13] show the same ship length curve behavior as wind speed increases for the same fixed values used by Vachon et al. (Figure 8). The unchanged beam parameters were Number of Looks (3.1), each mode incident angle, and azimuthal and range resolution. Figures 11,13,15 and 17 show the cumulative K-distributions for each case that were used to produce an critical intensity value for each mode.

Table 9 shows the comparison between Vachon et al. (1997) results and the results produced for this thesis. The differences in minimum detectable ship length are typically less than 5 m. Therefore the reproduction of the model is acceptable for the

main purpose of this thesis, the performance prediction for next generation ship detection spaceborne SAR.

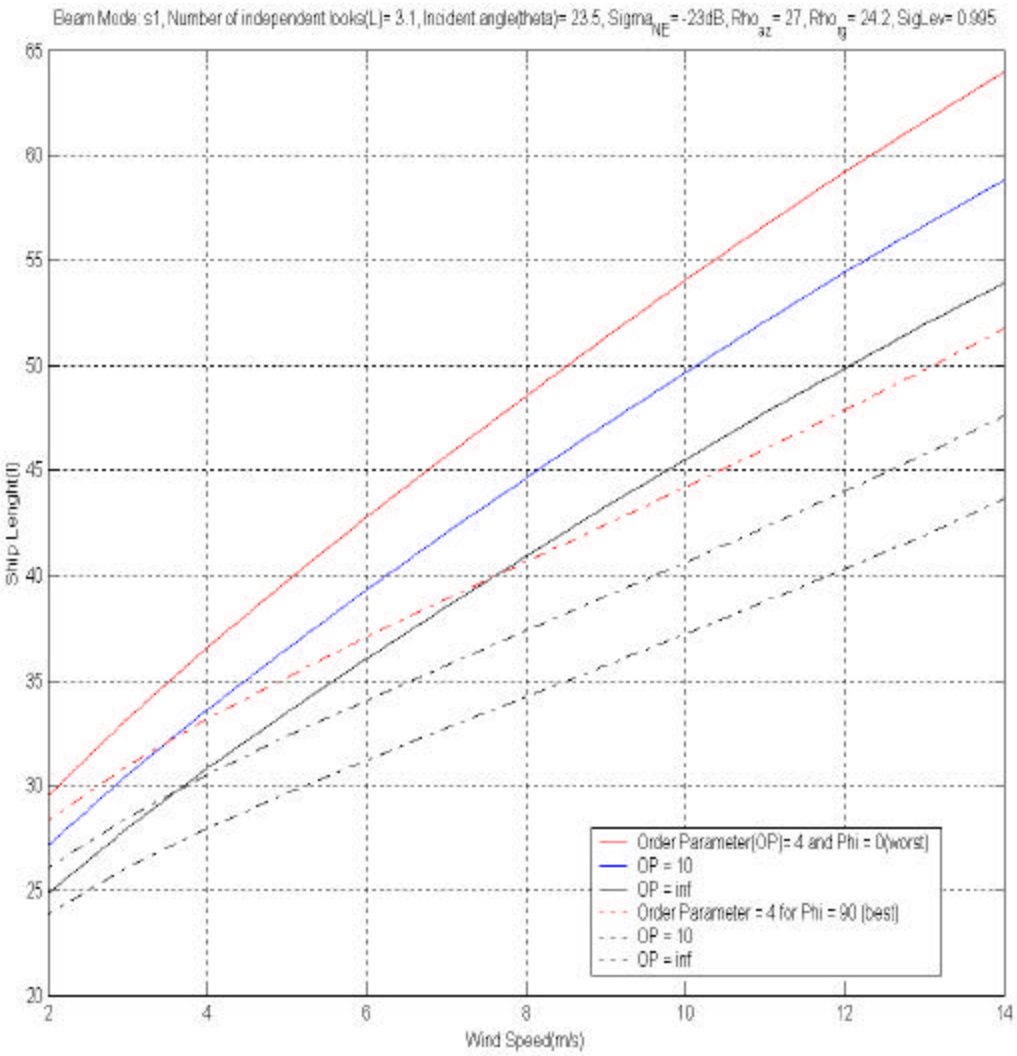

Figure 10. S1 mode 'Wind versus Ship' length thesis results

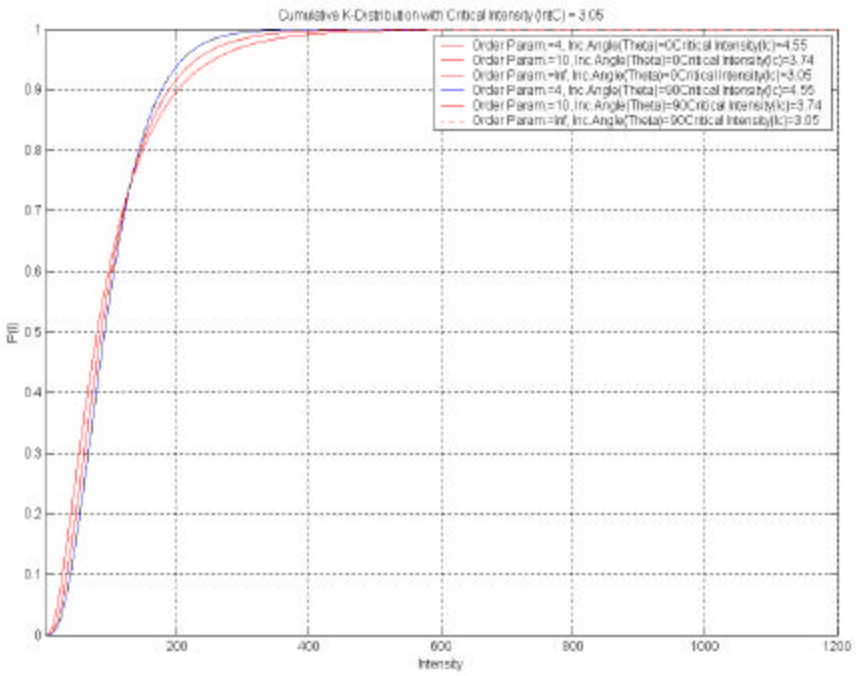

Figure 11. S1 mode Cumulative PDF with Critical Intensity Values

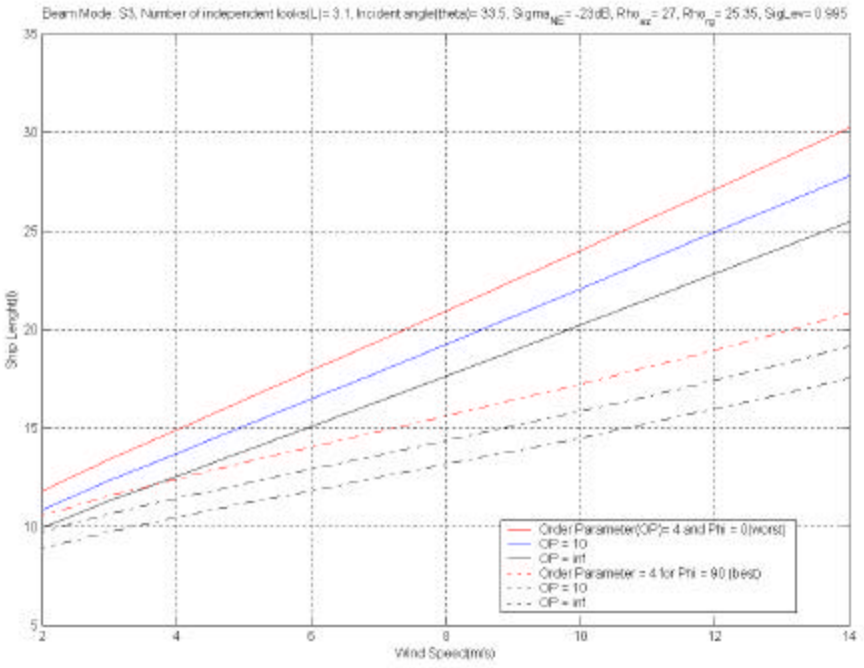

Figure 12. S3 mode 'Wind versus Ship' length thesis results

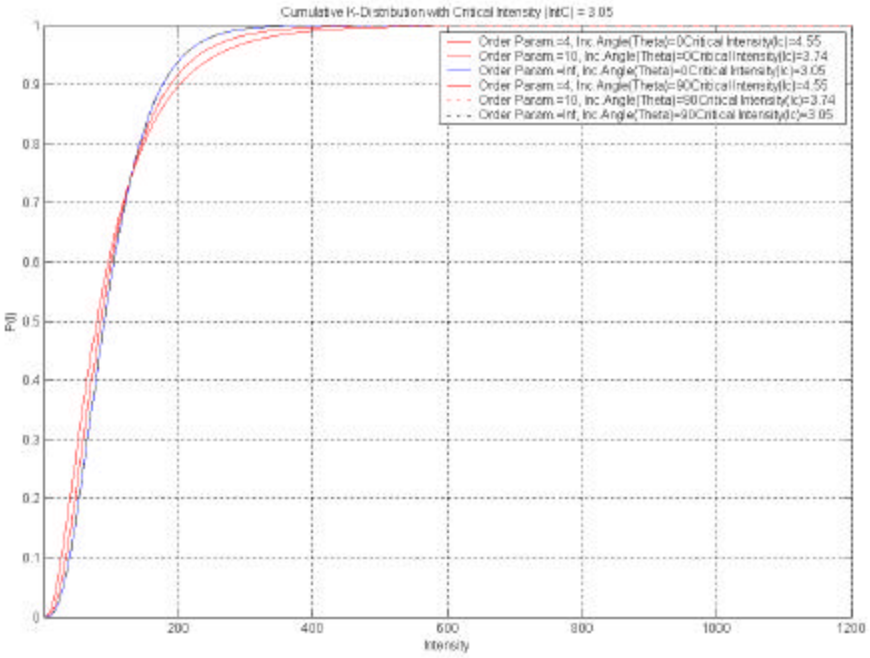

Figure 13. S3 mode Cumulative PDF with Critical Intensity Values

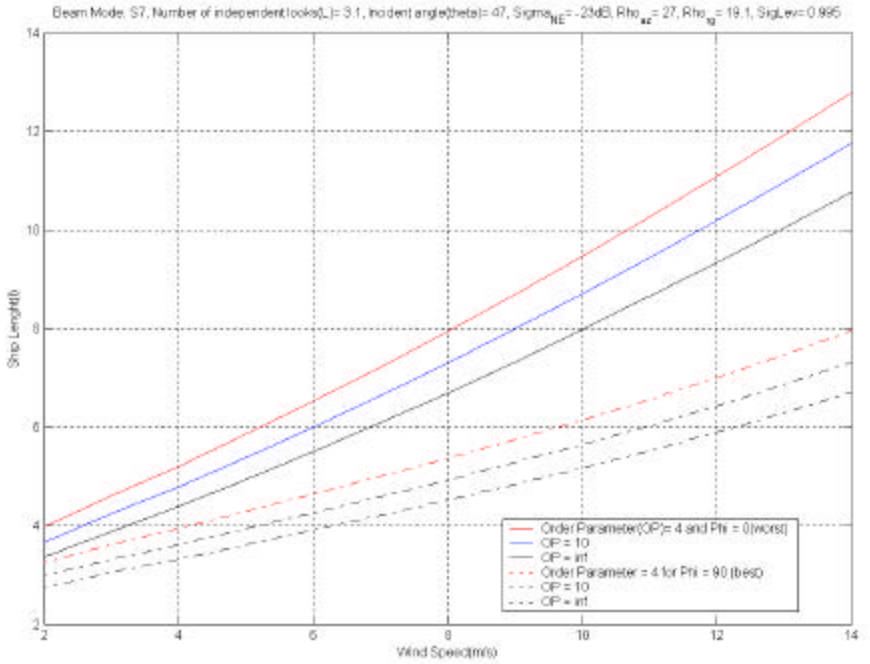

Figure 14. S7 mode ‘Wind versus Ship’ length thesis results

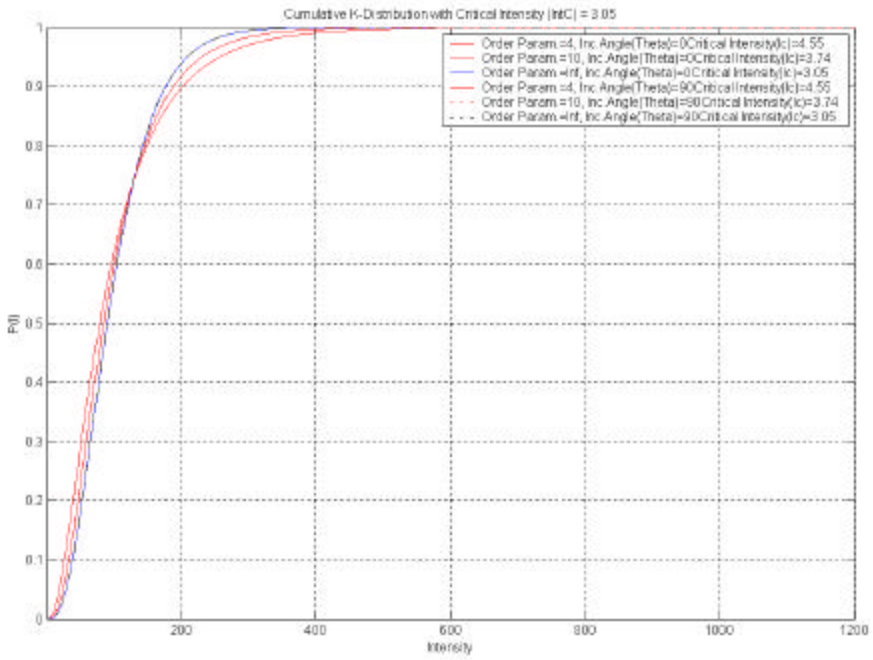

Figure 15. S7 mode Cumulative PDF with Critical Intensity Values

Table 9. Vachon versus thesis length differences for S1, S3, S7 and ERS modes

Obs.: Values rounded to meter and values computed for wind = 2 m/s

Modes	**$S1_v$**	**$S1_t$**	**$S1_v$- $S1_t$**	**$S3_v$**	**$S3_t$**	**$S3_v$- $S3_t$**
Worst	27	29	+2	13	12	-1
Best	20	24	-4	10	9	-1
Modes	**$S7_v$**	**$S7_t$**	**$S7_v$- $S7_t$**	**ERS_v**	**ERS_t**	**ERS_v- ERS_t**
Worst	9	4	-5	40	38	-2
Best	7	3	-4	28	30	+2

Worst is Upwind with Order Parameter=4; Best is Crosswind with Order Parameter = inf

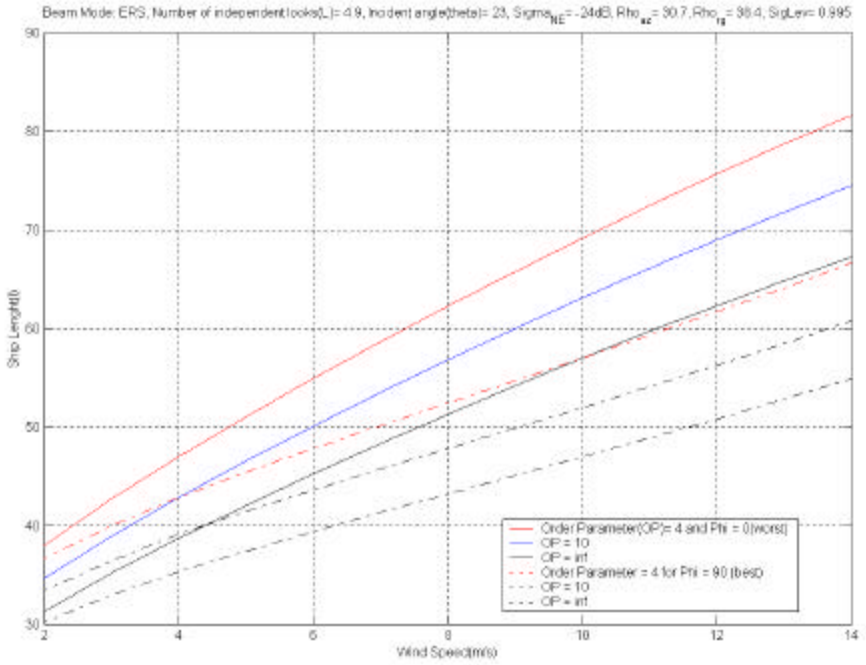

Figure 16. ERS 'Wind versus Ship' length thesis results

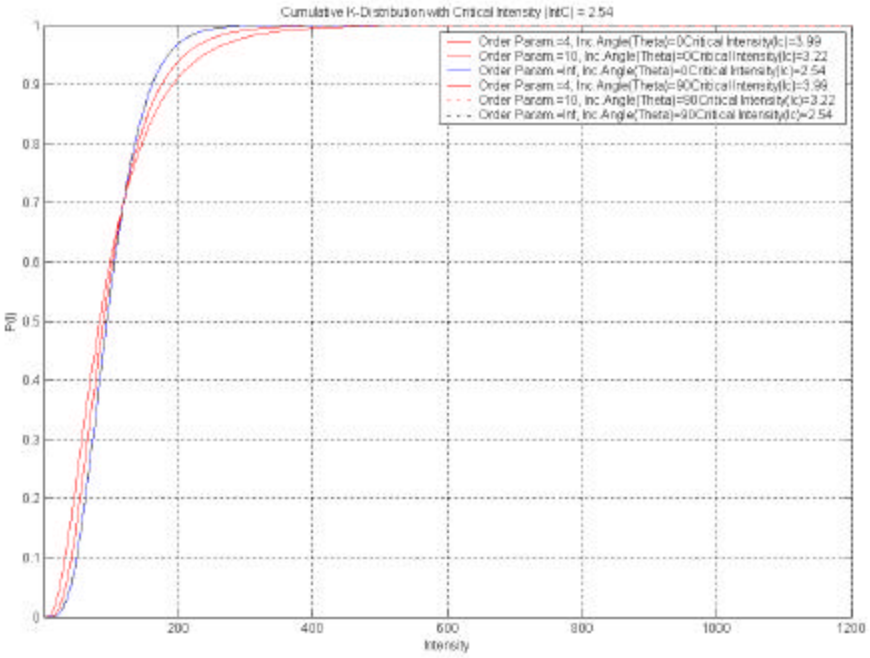

Figure 17. ERS mode Cumulative PDF with Critical Intensity Values

4. Expected Results for Fine Mode Resolution

Figures 18, 19 and 20 show the results using the RADARSAT-2 fine mode resolutions. The mean incident angle for each fine mode and the released Number of Looks, listed in Table 2, were used for each mode. All the Figures show the expected minimum ship length behavior as wind speed increases. Values with crosswind (best) and upwind (worst) conditions are shown with three different K-distribution order parameters. Despite the disadvantage of lack of coverage due to a small swath width, all expected detected ship length values associated with new high resolutions for fine modes (1.5 to 10 m) will lead not only to ship detection but also ship recognition.

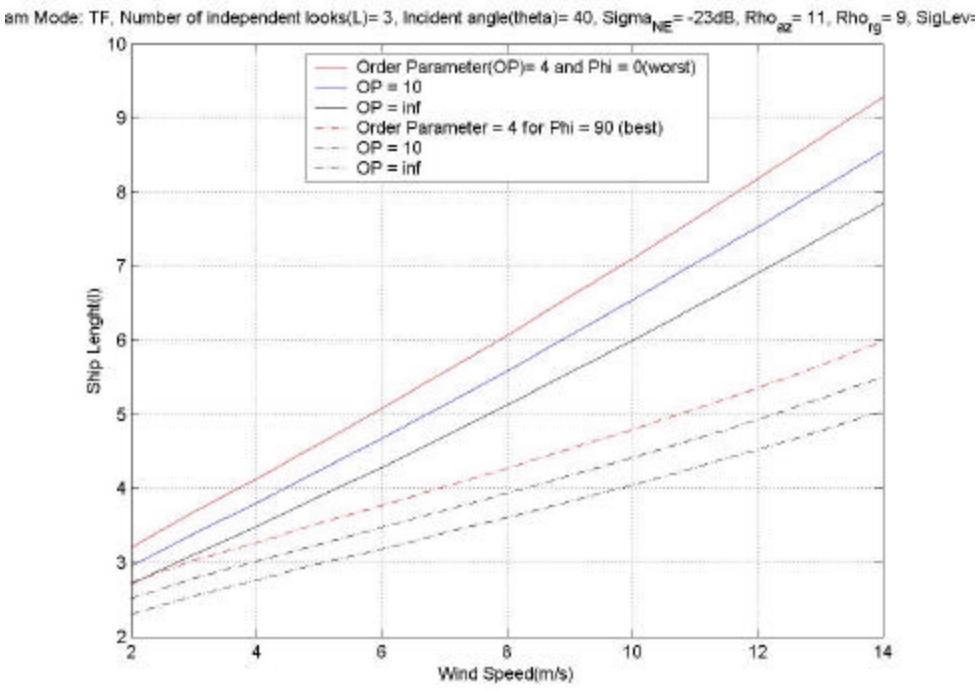

Figure 18. Ship length for RADARSAR 2 Triple Fine mode

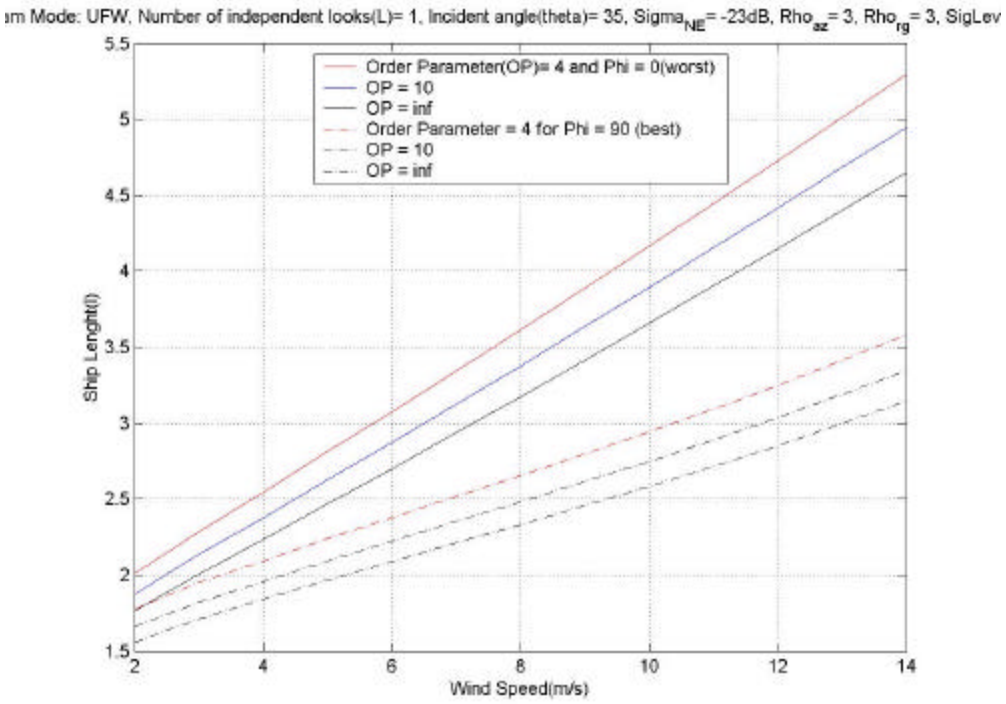

Figure 19. Ship length for RADARSAR 2 Ultra-Fine Wide mode

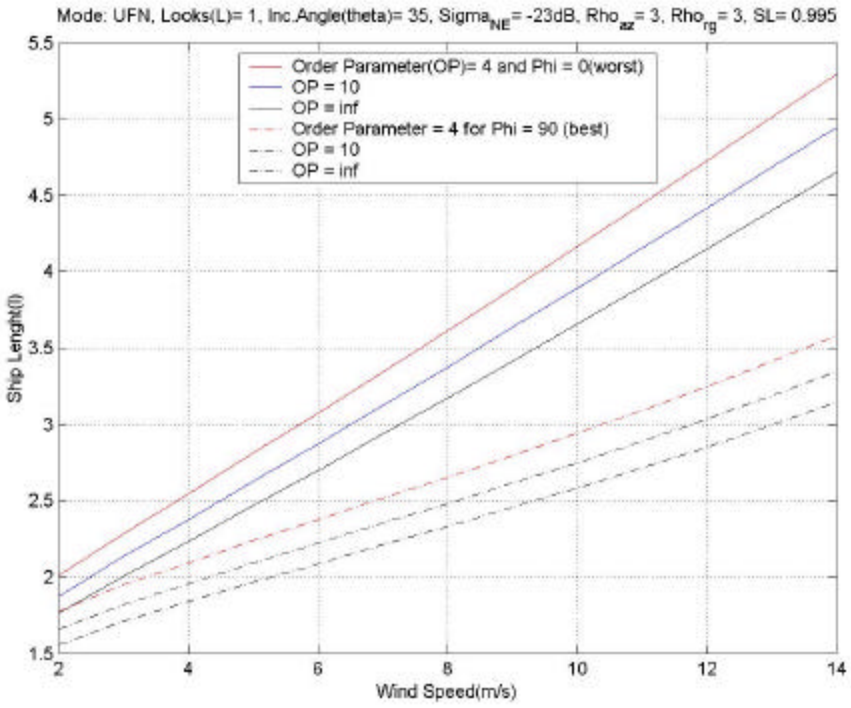

Figure 20. Ship length for RADARSAR 2 Ultra-Fine Narrow mode

5. Ship Length versus Resolution Qualitative Expected Behavior

Figure 21 shows how detectable ship length changes with a fixed wind velocity using one RADARSAR-2 mode (Standard), varying with resolution for upwind/crosswind (worst/best case), and with two Number of Looks values. Three major differences are noticeable. First, the high incidence angle detection can be increased in wide swath modes as much as five times compared to low incidence angle observations (ScanSAR narrow). Next, intermediate resolution modes (Standard), have less incident angle influence and almost the same influence of sea RCS and wind incident angle. Finally, at high resolution all three variables have about the same influence on final ship length computation.

6. Ship Length versus Incident Angle Qualitative Expected Behavior

Figure 22 shows the variation of detectable ship length versus incidence angle for a fixed wind velocity and RADARSAR mode (standard in this case) varying with resolution, upwind/crosswind (worst/best case) and Number of Looks. With an increasing incident angle the ship detectability increases by a factor of almost 2.5 for this specific case. High incident angle we have the best results for ship detection.

Figure 21 and 22 confirm the major role of resolution and incident angle in the Vachon et al. (1997) ship detection model. The effect of resolution decreases as the incident angle increases. Number of Looks and sensor-relative wind direction have a secondary, but not disregardable influence.

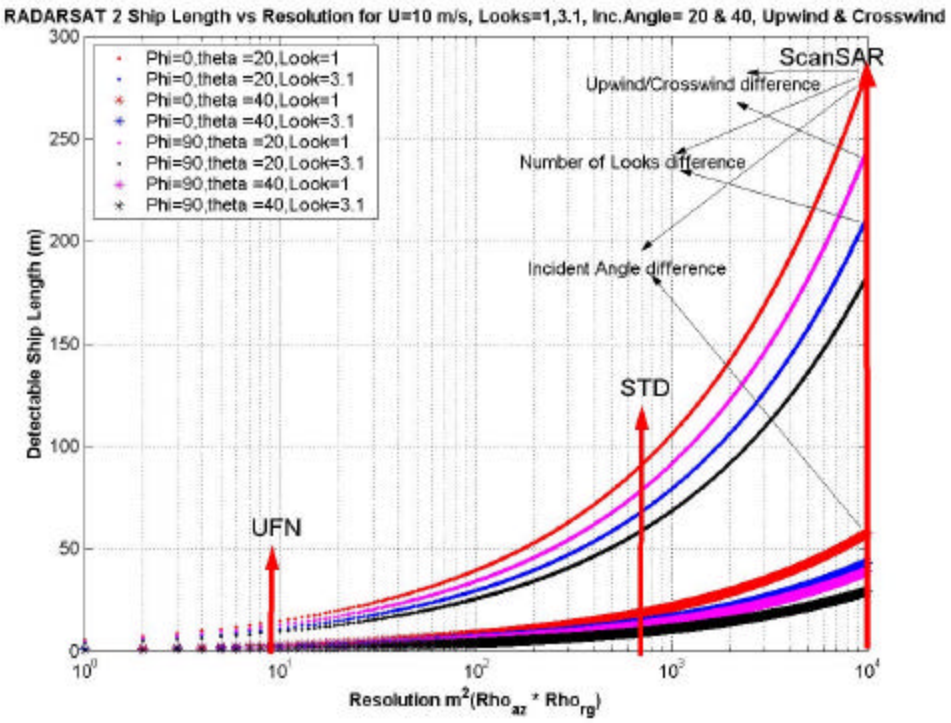

Figure 21. Ship Length versus Resolution Results

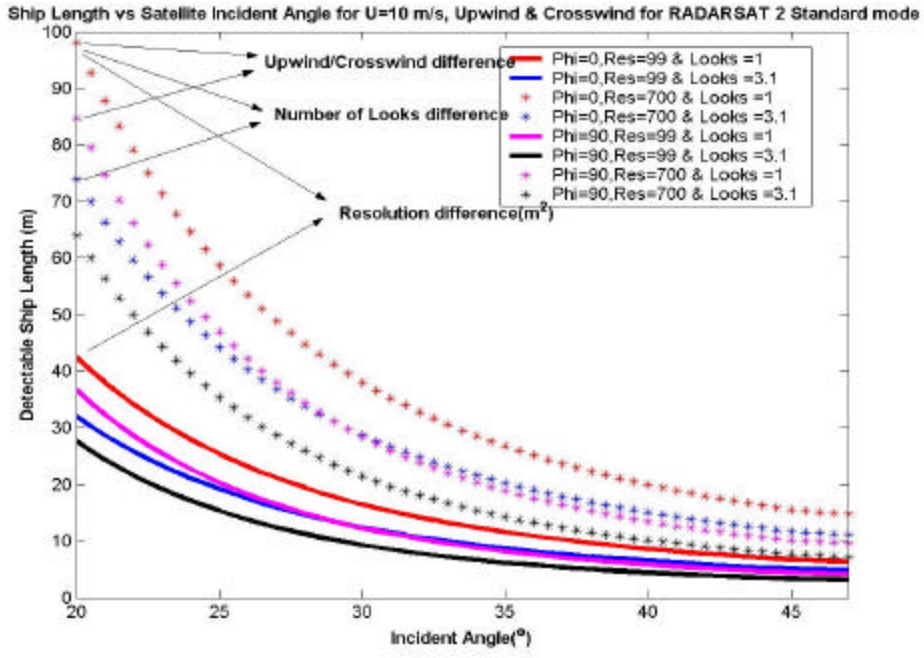

Figure 22. Ship Length versus Incident Angle Results

7. Practical Application

Given the wind condition as in Figure 23 at 0N, 34W and 4N, 34W (North Brazilian Coast) from PIRATA project, we can use the Vachon et al. (1997) model to estimate ship detection performance. For instance, using the same parameters and statistics as in the tested model for the S1 mode case on RADARSAT 2, we can expect that SAR images taken under the same conditions as in Figure 10 (mode wind velocity of 6 m/s), ship lengths from 32 to 43 (best and worst case) are expected to be detected. This short example testifies to the model's usefulness in analyzing real situations setting the best parameters for ship detection with RADARSAT 2.

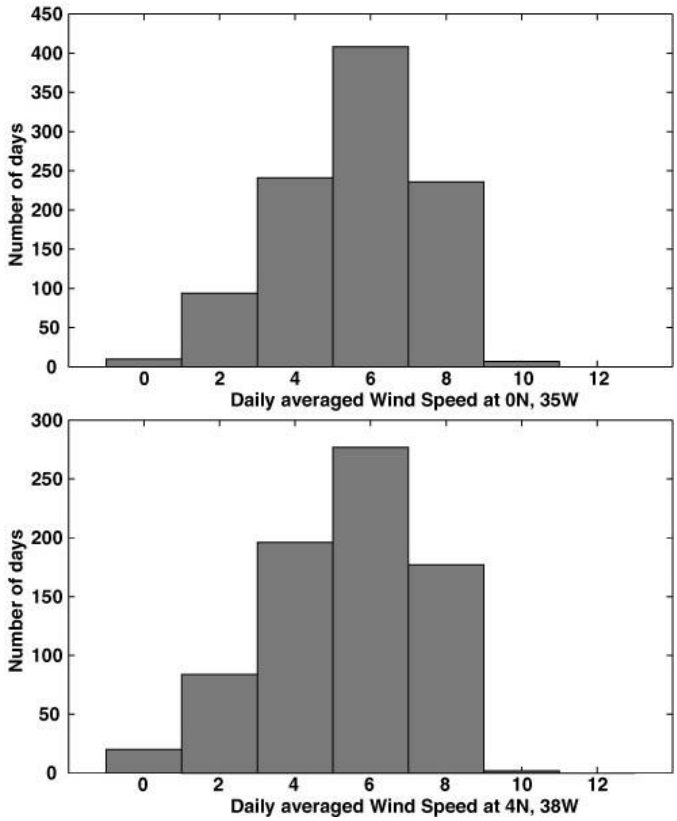

Figure 22. Wind histogram from PIRATA site

THIS PAGE INTENTIONALLY LEFT BLANK

V. CONCLUSIONS

The ship detection model outlined by Vachon et al. (1997) was used to verify and quantify ship detection improvements expected in the next generation spaceborne SAR imagery. This thesis focuses on the influence of incidence angle, wind speed and resolution, on the detectability of ships in SAR imagery. The results are compared to RADARSAT 2 parameters to test the improvement expected from new capabilities. The impact of new polarized modes in ship detection is not tested in this thesis.

Vachon et al. (1997) uses a model of the ocean Radar Cross Section (RCS) as a function of wind speed and incidence angle. The minimum ship length that can be detected against the background ocean radar cross section is determined by the critical intensity level obtained from a statistical relationship between ship size and RCS.

The minimum detectable ship length is strongly dependent on wind speed due to the changes imposed by the wind on RCS of the ocean and on the critical intensity. For instance in RADARSAT-2 S1 mode, with 3.1 Number of Looks, with 23.5° of incident angle with 99.5 % of confidence, we expect winds to change from 2 to 10 m/s while the detectable ship lengths change from 29m to 54m in the worst case and from 24m to 37m in the best case. For areas surveyed by the PIRATA project on the North Brazilian Coast (0N, 34W and 4N, 34W) with mode wind velocity of 6 m/s, minimum detectable ship lengths from 32 m to 43 m (best and worst cases) are expected to be detected.

The minimum detectable ship length changes dramatically with beam incident angle. The increase in incidence angle reduces Ocean RCS due to a reduction of Bragg

scatter to the sensor and the increase of the ship RCS due to an increase in double bounce scatter. For instance, for RADARSAT 2 standard mode, with 10 m/s wind speed in the worst case (upwind related to the antenna), increasing the incident angle from 20° to 45° changes the detectable ship length from 99m to 20m – nearly a factor of five change.

The minimum detectable ship length is strongly dependent on radar resolution since reduction of the pixel size increases the probability that photons from that pixel are reflected by the ship. For instance, changing modes in RADARSAT 2 from ScanSAR to UltrafineNarrow, thereby increasing resolution by a factor of 10^3 in area, with 10 m/s wind speed, 20° of incident angle and Number of Looks equal 1, the detectable ship length will decrease from 280m to 15m (worst case) – almost a factor 20 change.

The best ship detection results are obtained with RADARSAT 2 Fine Resolution Modes. The minimum detectable ship lengths of 1.5 to 3.5 meters for fine mode resolution not only illustrate the improvement of ship detection, but also make ship recognition possible given the right conditions. Additionally, ship recognition will be improved by cross polarization.

The general level of improvement for RADARSAT 2, ALOS/PALSAR and ENVI/ASAR arises from the new resolution modes and cross polarization. Some specific design factors should be mandatory for future SARs designed specifically for ship detection. High incident angles orbits, shorter repeat cycle, multipolarization and large swath width at high resolution are among the main SAR characteristics needed for future ship detection satellites.

LIST OF REFERENCES

AGARD, 1992**:** Fundamentals and special problems of synthetic aperture radar (SAR). *Advisory Group for Aerospace Research & Development (AGARD) lectur series,* **182.**

Copeland, A C, G. Ravichandran and M. M. Trivedi, 1995: Localized Radon Transform-Based Detection of Ship Wakes in SAR images. *IEEE trans. Geoscience and Remote Sensing,* **33**, 35-45.

Curlander, C. et al., 1992: Fundamentals and Special Problems of Synthetic Aperture Radar (SAR). *AGARD lecture series*, **182.**

Elachi, C., 1982: *Introduction to the Physics and Techniques of Remote Sensing.* John Wiley & Sons.

Franceschetti, G & Lanari, R, 1999: *Synthetic Aperture Radar processing*. CRC Press.

Gower, J.F.R , P.W Vachon and H. Edel, 1993: Ocean Applications of RADARSAT. *Canadian Journal of Remote Sensing,* **19**(4), 372-383.

Graham, L.C., 1974: Synthetic Interferometer Radar for Topographic Mapping. *Proc IEEE,***62**, 763.

Long, M.W, 2001: *Radar Reflectivity of Land and Sea-3.* Artech House Inc.

Oliver, C.J, 1993: Optimum texture estimators for SAR clutter. *J.Physics :* **D**, pp 1824-1835.

Oliver, Chris & Quegan, Shaun, 1998: *Understanding Synthetic Aperture Radar Images. Artech House*

Olsen, Richard B., P W.Vachon and Terje Wahl, 2000: Vessel Detection using SAR imagery: current status and some views for the future. *Canadian Centre for Remote Sensing Internet Bibliography Database*.

Rey, M T, A. Drosopoulos and D Petrovic, 1990: Application of Radon Transform Techniques to Wake Detection in Seasat-A SARimages. *IEEE Trans. Geoscience and Remote Sensing*, **28,** pp 553-560

Rey, Maria T. and Anastasios Drosopoulos, 1996: A Search Procedure for Ships in RADARSAT imagery (U). Defense Research Establishment Ottawa-Report n° 1305

Robinson, I.S, (1985): Satellite Oceanography – *An introduction for oceanographers and remote-sensing scientists.* John Wiley & Sons.

Skolnik, M.I, 2001: *Introduction to Radar Systems.* Ed. McGraw-Hill.

Snoeij, P., C.M.H. Unal and E.P.W. Attena, 1991: The Response of the Radar Echo from the Ocean Surface to the Surface Wind Vector at Frequencies Between 1 and 18 GHz Compared with Model Predictions, *Proceedings IGARSS'91, IEEE Publication,* **91.**

Stewart, R.H, 1985: *Methods of Satellite Oceanography*. University of California Press.

Stimson, G.W, 1998: *Introduction to Airborne Radar*. SciTech publishing.

Unal, C.M.H, P. Snoeij and P.J.F.Swart, 1991: The Polarization-Dependent Relation Between Radar Backscatter from the Ocean Surface and Surface Wind Vector at Frequencies Between 1 and 18 GHz. *IEEE transactions on Geoscience and Remote Sensing,* **29,** 621-626

Vachon, P. W., Campbell, J. W. M., Bjerkelund, C. A., Dobson, F. W., Rey M. T., 1997: Ship Detection by the RADARSAT SAR: Validation of Detection Model Predictions. *Canadian Journal of Remote Sensing,* **23** ,48-59.

Vachon, P.W., S.J. Thomas, J. Cranton, H.R. Edel and M.D. Henschel, 2000: Validation of Ship Detection by the RADARSAT Synthetic Aperture Radar and the Ocean Monitoring Workstation. *Canadian Journal of Remote Sensing,* **26 ,** 200-212.

APPENDICES

A. UNAL'S TABLE INTERPOLATION CODE

```
function [Pr_Interpol_in_dB] = UnalsInt(V,theta,IntModeType)
%*************************************************************
% Interpolation to find Unal's et al. tabulated polarization ratio
%*************************************************************

% inputs

%     V - the wind speed in m/s
%     theta - the incidence angle in degrees
%     IntModeType – Matlab interpolation type, ie, 'linear','cubic',etc

% output

%     Pr_Interpol_in_dB = Polarization Ration Interpolated in decibels

Beam_Inc_Tb= [20 30 45 47]'
Spd_Wind_Tb= [2 4 6 8 10 12 14]

% Unal's et al., table values in dB extrapoleted until 47 degrees

PRu=[ 1.05 2.07 4.78 4.48
      0.79 2.37 5.25 5.25
      0.65 2.57 5.47 5.47
      0.56 2.70 5.59 5.59
      0.51 2.80 5.66 5.66
      0.49 2.88 5.71 5.71
      0.49 2.95 5.75 5.75]';

%Polarization Ratio in dB

Pr_Interpol_in_dB = interp2(Spd_Wind_Tb,Beam_Inc_Tb,PRu,V,theta,…
IntModeType);
```

B. CMOD-IFR2 IFREMER MODEL CODE FROM CCRS

```
% function sigma0 = ifremer(V,phi,theta);
% calculate radar cross-sections for cmod3 model wind retrieval
% algorithm according to IFREMER off-line analysis
% inputs
%     V - the wind speed in m/s
%     phi - the relative radar look-wind in degrees...this angle is
%           zero whe nthe wind is blowing towards the radar
%     theta - the incidence angle in degrees
% output
%     simga0 - radar cross-section (linear units)
c = [-2.437596 -1.567030   0.370824
      -0.039714  0.410275   0.184862
      -0.026785  0.130832  -0.466007
      0.192522  -0.027294   0.032854
      0.003595  0.073938   0.12845
      0.012663  0.044884   0.004448
      -0.007864  -0.001635];
x = (theta - 36)./19;
p0 = 1;
p1 = x;
p2 = (3.*x.^2 - 1)./2;
p3 = (5.*x.^2 - 3).*x./2;
alpha = c(1) + c(2).*p1 + c(3).*p2 + c(4).*p3;
beta  = c(5) + c(6).*p1 + c(7).*p2;
delta = c(8) + c(9).*p1 + c(10).*p2;
b0 = 10.^(alpha + beta.*sqrt(V - delta));
b1 = c(11) + c(12).*p1 + c(13).*V;
b2 =  c(14) + c(15).*p1 + c(16).*p2 + (c(17) + c(18).*p1 + c(19).*p2).*V
+ c(20).*V.^2;
sigma0 = b0.*(1 + b1.*cos(phi.*pi/180) + b2.*cos(2.*phi.*pi/180))
```

C. INTERNET SITES:

CCRS/RADARSAT, http://www.ccrs.nrcan.gc.ca/ccrs/tekrd/radarsat/rsate.html/
ENVISAT/ASAR, http://envisat.estec.esa.nl/instruments/asar/
ALOS/PALSAR, http://alos.nasda.go.jp/index-e.html
JPL/NASA, http://southport.jpl.nasa.gov/desc/imagingradarv3.html
PIRATA, http://www.brest.ird.fr/pirata/pirataus.html

INITIAL DISTRIBUTION LIST

1. Defense Technical Information Center
   8725 John J Kingman Rd.,STE 0944
   Ft. Belvoir, VA ,22060-6218

2. Dudley Knox Library
   Naval Postgraduate School
   411, Dyer Rd.
   Monterey, CA, 93943-5101

3. CDR James A. Hill
   Naval Postgraduate School
   Monterey, CA 93943-5000

4. Chairman, Department of Oceanography
   Naval Postgraduate School
   Monterey, CA 93943-5000

5. Chairman, Department of Meteorology
   Naval Postgraduate School
   Monterey, CA 93943-5000

6. Professor Philip A. Durkee, MR/De
   Naval Postgraduate School
   Monterey, CA 93943-5000

7. Professor Jeffrey D. Paduan, OC/De
   Naval Postgraduate School
   Monterey, CA 93943-5000

8. Professor Richard B. Olsen, Ph/De
   Naval Postgraduate School
   Monterey,CA 93940-5000
9. Canada Centre for Remote Sensing
   Paris W. Vachon, PhD
   588 Booth St. Room 353
   Ottawa, Ontario, Canada K1A 0Y7

10. Brazilian Navy
    Diretoria de Hidrografia e Navegação
    Rua Barão de Jaceguai s/n – Ponta da Armação
    Niterói, RJ, 24048-900

11. Brazilian Navy
Centro de Hidrografia da Marinha
Rua Barão de Jaceguai s/n – Ponta da Armação
Diretoria de Hidrografia e Navegação
Niterói, RJ, 24048-900